Chapter 3
Scintillation Detectors for Charged Particles and Photons

P. Lecoq

3.1 Basic Detector Principles and Scintillator Requirements

3.1.1 Interaction of Ionizing Radiation with Scintillator Material

As any radiation detector, a scintillator is an absorbing material, which has the additional property to convert into light a fraction of the energy deposited by ionizing radiation. Charged and neutral particles interact with the scintillator material through the well-known mechanisms of radiation interactions in matter described by many authors [1, 2]. Charged particles continuously interact with the electrons of the scintillator medium through Coulomb interactions, resulting in atomic excitation or ionization. Neutral particles will first have to undergo a direct interaction with the nucleus producing recoil protons or spallation fragments, which will then transfer their energy to the medium in the same way as primary charged particles.

The rate of energy loss ($-dE/dx$) for charged particles is strongly energy dependant. It is well described by the Bethe-Bloch formula (see Chap. 2) for incoming particles in the MeV-GeV range, with atomic shell corrections at lower energy and radiative loss corrections at higher energy. For heavy materials currently used as scintillators with a density of 6–8 g/cm^3, it is typically of the order of 10 MeV/cm for a minimum ionizing particle but it can be a factor up to 100 more at very low or very high energy (radiative losses).

P. Lecoq (✉)
CERN, Geneva, Switzerland
e-mail: Paul.Lecoq@cern.ch

In the case of X- or γ- rays, the three fundamental mechanisms of electromagnetic interaction are [3]:

- Photo-absorption
- Compton scattering
- Electron-positron pair production

The dominant process at low energy (up to a few hundred keV for heavy materials) is the photoelectric absorption. The interacting photon transfers its energy to an electron from one of the electron shells of the absorber atom (usually from a deep shell). The resulting photoelectron is ejected with a kinetic energy corresponding to the incident photon energy minus the binding energy of the electron on its shell. This is followed by a rapid reorganization of the electron cloud to fill the electron vacancy, which results in the emission of characteristic X-Rays or Auger electrons. The photoelectric process has the highest probability when the incident photon has an energy comparable to the kinetic energy of the electron on its shell. This is the origin of the typical peaks observed in the cross-section curve corresponding to resonances for the different electron shells (Fig. 3.1). The general trend of this cross-section is a rapid decrease with energy and a strong dependence on the atomic number Z of the absorber explaining the preponderance of high-Z materials for X- or γ-rays detection and shielding:

$$\sigma_{ph} \propto \frac{Z^5}{E_\gamma^{7/2}} \tag{3.1}$$
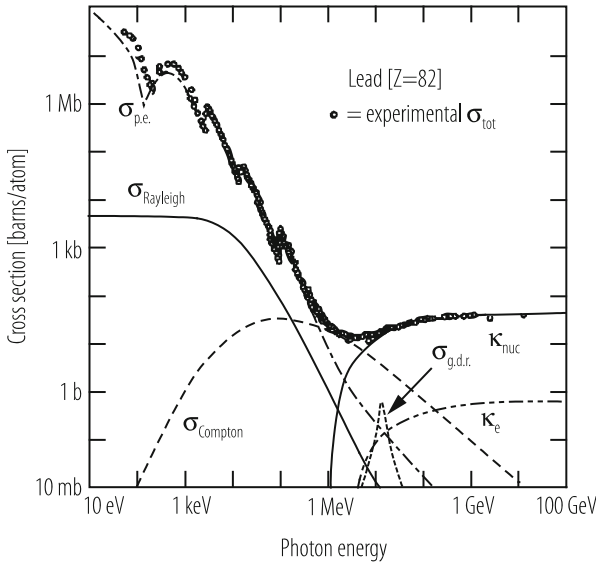
Fig. 3.1 Energy dependence of photon total cross sections in Lead (from Particle Data Group)

At energies above a few hundred keV, Compton scattering becomes predominant. In this case, the incident photon transfers only part of its initial energy E_γ to an electron of the atomic shells and is scattered at an angle θ with respect to its original direction. The recoil electron is then rapidly absorbed by the scintillator and releases an energy according to the formula:

$$E_{\mathrm{e}} = E_\gamma - E'_\gamma - E_{\mathrm{ebinding}} \tag{3.2}$$

where E'_γ is the energy of the scattered photon given by (with m_0 the rest mass of the electron):

$$E'_\gamma = \frac{E_\gamma}{1 + \frac{E_\gamma}{m_0 c^2}\,(1 - \cos\theta)} \tag{3.3}$$

The energy released in the scintillator by the recoil electron is distributed on a continuum between zero and a maximum up to $E_\gamma - m_0 c^2/2 = E_\gamma - 256$ keV (for gamma energy large compared to the rest mass of the electron).

The probability of Compton scattering is related to the electron density in the medium and increases linearly with the atomic number of the absorber, favouring therefore high Z materials.

Above a threshold of 1.02 MeV (twice the rest mass of the electron), the mechanism of e^+e^- pair production can take place, predominantly in the electric field of the nuclei, and to a lesser extent in the electric field of the electron cloud (respectively κ_{nuc} and κ_{e} in Fig. 3.1). Similarly to photo-absorption and Compton scattering this process has a higher probability for high Z materials as the cross section is approximately given by the formula [4]:

$$\sigma_{\mathrm{pair}} \propto Z^2 \ln\left(2E_\gamma\right) \tag{3.4}$$

Below the threshold of electron-positron pair production electrons will continue to loose energy mainly through Coulomb scattering.

In the case of an ordered material like a crystal another mechanism takes place at this stage. In the process of energy degradation the electrons in the keV range start to couple with the electrons of the atoms of the lattice and excite the electrons from the occupied valence or core bands to different levels in the conduction band. Each of these interactions results in an electron-hole pair formation. If the energy of the electron is high enough to reach the ionization threshold free carriers are produced, which will move randomly in the crystal until they are trapped by a defect or recombine on a luminescent centre. In the case the ionization threshold is not reached the electron and hole release part of their energy by coupling to the lattice vibration modes until they reach the top of the valence band for the hole and the bottom of the conduction band for the electron. They can also be bound and form an exciton whose energy is in general slightly smaller than the bandgap between the valence and the conduction bands. At this stage the probability is maximum

for their relaxation on luminescent centres through an energy or a charge transfer mechanism.

For a material to be a scintillator it must contain luminescent centres. They are either extrinsic, generally doping ions, or intrinsic i.e. molecular systems of the lattice or of defects of the lattice, which possess a radiative transition between an excited and a lower energy state. Moreover, the energy levels involved in the radiative transition must be smaller than the forbidden energy bandgap, in order to avoid re-absorption of the emitted light or photo-ionization of the centre.

In a way, a scintillator can be considered as a wavelength shifter. It converts the energy (or wavelength) of an incident particle or energetic photon (UV, X-ray or gamma-ray) into a number of photons of much lower energy (or longer wavelength) in the visible or near visible range, which can be detected by photomultipliers, photodiodes or avalanche photodiodes.

## 3.1.2 Important Scintillator Properties

Scintillators are among the most popular ionizing radiation detectors.

There are two main classes of scintillators: inorganic and organic. For the inorganic systems (generally ionic crystals), scintillation arises from thermalized electrons and holes, moved to the bottom of the conduction band or the top of the valence band respectively, by scattering from the initially produced fast charge carriers. For the organic systems, scintillation arises upon transition between an excited molecular level and the corresponding electronic ground state. Inorganic scintillators are generally brighter but with a slower decay time than organic ones. However no "ideal" material exists and the choice of a scintillator depends on the application, as it is generally driven by a trade-off between a number of physico-chemical and optical parameters such as density, scintillation properties and radiation hardness. The production and processing cost is also an important issue taking into consideration the very large volumes required for some applications.

3.1.2.1 Physico-chemical Properties

Physico-chemical properties are related to the material composition, structure and density, as well as to its chemical stability when exposed to different environmental conditions: air, humidity, ionizing radiation.

Frequently the density and hence the compactness of the detector is essential in order to reduce the detector volume and cost. This is achieved by using high stopping power and therefore high density materials. This reduces the size of the shower for high energy γ's and electrons as well as the range of Compton scattered photons for lower energy γ-rays. A dense material also reduces the lateral spread of the shower, which is particularly important for the majority of High Energy Physics detectors.
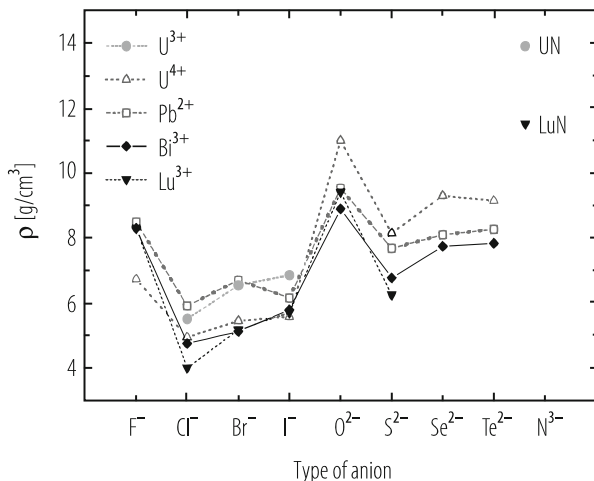
Fig. 3.2 Density for various binary compounds as a function of the binding anion (courtesy P. Derenbos, from ref. [5])

Crystals with a density higher than 8 g/cm^3 are currently available, such as Lead Tungstate (PWO: 8.28 g/cm^3) or Lutetium Aluminium Perovskite (LuAP: 8.34 g/cm^3). Materials of even higher density in the range of 10 g/cm^3 are being identified and studied, such as: Lutetium Oxide: Lu_2O_3, Lutetium Hafnate: $Lu_4Hf_3O_{12}$, Lutetium Tantalate: Lu_3TaO_7, Lutetium Lead Tantalate: $LuPb_2TaO_6$, Thorium Oxide: ThO_2. Scintillators are wide bandgap ionic materials and high density implies the choice of anions and cations of high atomic number A (and therefore high Z), as well as small ionic radius to increase the ionic density in the crystal lattice. From this point of view, oxides are generally denser than iodides because of the much smaller ionic radius of the oxygen compared to the iodine ion and in spite of its lighter weight. Similarly, the oxidation potential of the anion is important as it allows reducing the number of anions (generally light) needed to compensate for the positive charge of the much heavier cation. For this reason oxygen is a better ligand than the slightly heavier fluorine ion because of its higher oxidation state (2 or 3 instead of 1). Figure 3.2 illustrates this effect for a number of binary compounds as a function of the anion type.

High Z materials are also preferred for low and medium energy spectroscopy because of the strong dependence of the photoelectric cross-section on Z (see Sect. 3.1.1). High density is also required at high energy to achieve a small radiation length X_0 (mean distance over which an electron loses 1/e of its energy) given as a function of the density ρ, atomic mass A and atomic number Z by:

$$X_0 = \frac{A}{\rho} \frac{716.4 \mathrm{gcm}^{-2}}{Z\,(Z+1)\ln(287/Z)} \tag{3.5}$$

However, contrary to a common assumption, the optimum conditions are not necessarily achieved with the highest Z ions, because in addition to a small X_0, the density ρ should be high. This reduces the lateral shower size given by the Moliere radius:

$$R_{\mathrm{M}} \approx X_0 \cdot (Z + 1.2) / 37.74 \sim 1/\rho \tag{3.6}$$

The stability of the physico-chemical parameters is also important for the detector design. Scintillation crystals are very stable materials, at least in the bulk, if grown under conditions allowing a good structural quality. This provides a high degree of internal symmetry in the material together with high energetic stability. However, the charge unbalance on the surface can be at the origin of different problems, such as a concentration of impurities or crystallographic defects. As a result, the material can interact with its environment and locally change its properties. The majority of halide crystals have the anions weakly bound to the cations at the surface. They are therefore easily replaced by OH^- radicals from the atmosphere, which have strong optical absorption bands in the visible spectrum. This causes a progressive brownish discoloration of the crystal surface, a well know feature of hygroscopic materials. Encapsulating the crystal in an inert atmosphere avoids this effect.

3.1.2.2   Optical Properties

Inorganic scintillators usually show wide emission bands because of multi-site emission centres differently distorted by the crystal field, as well as by temperature broadening of the optical transitions through vibronic coupling of the emission centres with the crystal lattice. These emission bands are situated in the optical window of the scintillator and produce light in the visible, near infrared or near ultraviolet part of the spectrum. One of the objectives of scintillator development is to design scintillators with emissions peaks matching the maximum quantum efficiency of photodetectors, typically 250–500 nm for photomultipliers and 450–900 nm for solid state photodetectors (pin diodes and avalanche photodiodes).

Light yield (LY) is an essential parameter for a scintillator as it directly influences the energy resolution at low or medium energy through the photostatistic term proportional to $(LY)^{-1/2}$ and the timing resolution proportional to $(\tau_{\mathrm{sc}}/LY)^{-1/2}$, with τ_{sc} being the scintillation decay time. The scintillation mechanism is a multi-step process, which will be described in detail in Sect. 3.2. The overall scintillation yield is determined by the product of efficiencies for all these steps. The dominant factor, which sets the fundamental limit on the light output of a given scintillator, is the number n_{eh} of thermalized electron-hole pairs (active for scintillation) produced in the ionization track of the incoming particle:

$$n_{\mathrm{eh}} = \frac{E_\alpha}{\beta \cdot E_{\mathrm{g}}} \tag{3.7}$$
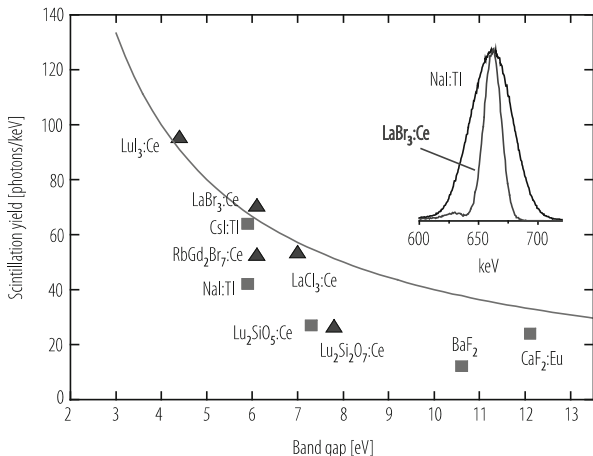
Fig. 3.3 Photon yield/keV of several scintillators as a function of the width of the forbidden band (courtesy P. Dorenbos)

where $\beta \cdot E_g$ is the mean energy necessary for the formation of one thermalized electron-hole pair in a medium with a forbidden zone of width E_g and E_α is the absorbed energy. For ionic crystals, the factor β is usually close to 2.3 and takes into account the energy loss through coupling with lattice phonons during the thermalization process [5]. As shown on Fig. 3.3 low bandgap materials have higher scintillation yields, although such materials are potentially more subject to trap induced quenching, re-absorption phenomena and photo-ionization of the luminescence centre. The ultimate light yield obtained for a material having a bandgap of 3 eV and an emission wavelength of about 600 nm is in the range of 140 photons/keV. The observed signal in photoelectrons/MeV is much smaller, due to losses in the light transport to the photodetector and the quantum efficiency of the photodetector.

The scintillation kinetics is another important consideration as a fast response and low dead time is frequently required for high detection rates. It is related to the rate of decrease of the population of the excited luminescent centres. For a simple process, with only one radiating centre and no interaction between luminescent centres and traps, the decay is exponential and characterized by a time constant τ_{sc}, the time after which the population has decreased by a factor e. For two independent radiating centres the same description with two exponentials holds. Real cases are however very often more complex, involving energy transfer between centres and quenching mechanisms, and the resulting light emission is strongly non-exponential. It is nevertheless common practice to describe this complex emission curve by a sum of exponentials with different time constants. This has in most of the cases no physical justification but simplifies the calculations. If we assume a very fast transfer of the electrons and holes to the luminescent centres the ultimate

limit for the scintillation decay time is given by the transition probability between its excited and ground states:

$$\Gamma = \frac{1}{\tau_{sc}} \propto \frac{n}{\lambda_{em}^3} \left(\frac{n^2+2}{3}\right)^2 \sum_f |\langle f| \mu |i\rangle|^2 \tag{3.8}$$

where n is the refractive index of the crystal, λ_{em} the emission wavelength of the transition, f and i the wave functions of the final and initial states respectively. The strength of the dipole operator μ connecting the initial and final state determines the decay time of the transition. This matrix element can only be sufficiently large for a transition between two states with different parity (parity allowed transition). This is in particular the case for the 5d to 4f transition in commonly used activators like Ce^{3+}, Pr^{3+}, Nd^{3+} and Eu^{3+}. Forbidden transitions are generally characterized by long decay times, unless a competitive non-radiative relaxation channel exists, which will contribute to the decrease of the population of excited states:

$$\frac{dn_e}{dt} = -\frac{n_e}{\tau} - \alpha n_e e^{-\frac{E}{kT}} \tag{3.9}$$

Here n_e represents the electronic density of the excited state, which is depopulated through two competing decay channels, the first one radiative with a rate $1/\tau$ and the second one, non-radiative, through a thermal quenching mechanism. E is the thermal energy barrier and α expresses the balance between the two channels. Fast scintillation can therefore be obtained for intrinsically slow transitions at the expense of a loss in light output. This is the case of Lead Tungstate (PWO) with a low light yield but 10 ns decay time at room temperature to be compared to a 25 times larger light yield but 6 μs decay time at 80°K [6]). More details about thermal quenching will be given in Sect. 3.2.

Special attention must be given to afterglow, which limits the counting rate of scintillation detectors. Afterglow is a phosphorescence mechanism induced by the thermal release of charge carriers from traps. These carriers will eventually recombine on luminescence centres, causing a delayed luminescence, which can reach several percent after 1 ms for NaI(Tl) or CsI(Tl). Other crystals have a much lower level of afterglow, such as BGO (Bismuth Germanate): 0.005% after 3 ms, and CsF (Cesium Fluoride): 0.003% after 6 ms [7].

3.1.2.3   Radiation Hardness

Inorganic scintillators have in general a good stability of their scintillation properties even in the presence of intense ionizing radiation environment. This property is crucially important for detectors in space, oil well logging and high-energy physics experiments at high luminosity accelerators. The radiation hardness of the scintillation mechanism is related to the strong electrostatic field of the crystal

lattice, which shields the luminescent centres. However, the transport of light through the crystal may be affected by the production of colour centres, which absorb part of the scintillation light on its way to the photodetector. The formation of colour centres results from the trapping of electric charges by crystal structural defects or impurities and is therefore directly correlated to the quality of the raw material and of the growth technology. A large effort is needed to purify the raw materials to the required quality and to minimize the amount of structural defects during the crystal growth. However, in some cases, a specific doping of the crystal has proven to be an efficient and economical way of significantly increasing the radiation hardness [8].

3.1.3 Scintillator Requirements for Various Applications

The choice of a scintillator depends on the energy of the ionizing radiation to be detected and on constraints specific to the application. It is therefore tailored to the user requirements considering the relative importance of several parameters, such as density, light yield, scintillation kinetics, emission spectrum, radiation hardness. Ruggedness, hygroscopic behaviour and production cost are also important parameters. In practice, it is impossible to find a scintillator, which combines all the most desirable properties. Besides a number of industrial applications for process control, container inspection, thickness gauging, ore processing and oil well logging a large fraction of the scintillator market is driven by X-ray and γ-ray spectroscopy in the following areas:

- High and medium energy physics particle detectors;
- Astrophysics and space applications;
- Spectrometry of low energy γ-quanta;
- Medical imaging;
- Safety Systems and Homeland Security.

The most important user requirements for each of these categories are detailed below.

3.1.3.1 High and Medium Energy Physics Particle Detectors

Scintillators are used in High Energy Physics for compact, high precision, homogeneous electromagnetic calorimetry. The purpose is to measure with the highest achievable precision the energy of electrons and photons, generally the decay products of unstable heavier particles, over the widest possible energy range.

The first important requirement is a high density material. High energy implies a high particle multiplicity of the particle collisions and requires a high granularity with good lateral containment of the particle initiated showers in order to minimize overlapping showers and to ease event reconstruction. A small Moliere radius is

therefore required, which will also improve the electron identification and allow π^0 rejection with good efficiency in high multiplicity events. More generally, a high stopping power is mandatory to longitudinally contain high energy showers in a reasonable volume and cost (typically 20–25 X_0 are needed in high energy calorimeters to contain at least 95% of the shower). Total lateral and longitudinal containment of the showers is a prerequisite to minimize leakage fluctuations and to achieve good energy resolution.

Fast scintillation is also an important parameter. In the search for rare events, and at hadron colliders, one operates at high collision rates, which requires a short time response of the detectors. Decay times of the order of the bunch crossing time (typically 25 ns) or even less are necessary. Only optically allowed (inter-configuration) transitions (like the transition 5d → 4f for Ce^{3+}), cross-luminescence, which is intrinsically fast and temperature independent as observed in Barium Fluoride (BaF_2), and strongly quenched intrinsic luminescence (as for PWO) can give rise to a fast light signal.

The demand for a high light yield is less stringent at high energy (GeV range) than at low energy (MeV range), because of the high number of scintillation photons produced even by a poor scintillator, allowing a good signal detection above the electronic noise. Such low light yield scintillators can therefore also be used for calorimetric applications in magnetic spectrometers due the rapid development of silicon photomultipliers (SiPM), with a gain comparable to photomultiplier tubes (PMT) and with the additional advantages of being very compact and immune to strong magnetic fields.

However, the high track density and event pile-up at high luminosity colliders pose serious challenges for physics event reconstruction and analysis. At the Large Hadron Collider (LHC) at CERN up to 40 pile-up events and more can be produced at each bunch crossing at the design luminosity of 2.10^{34} cm^{-2} s^{-1}, which will reach 200 pile-up events when the luminosity will be increased to 10^{35} cm^{-2} s^{-1} at the High Luminosity LHC [9]. For a collision region of about 10 cm (bunch length) the collisions will be distributed over 300 ps (Fig. 3.4 left panel). Precise temporal association of collision tracks or jets would help mitigate the pile-up. If this can be done for charged particles at high transverse momentum with particle tracking detectors this approach will be much more difficult in the forward-backward region and even impossible for neutral particles. In this case only time-of-flight (TOF) techniques can be applied as shown on the right panel of Fig. 3.4, where the two crossing bunches are symbolized by blue and red bars while their overlapping area is represented by a white bar. Events generated in the centre of the detector ($z = 0$) will generate tracks arriving at the same time in the forward and backward regions. On the other hand, events generated at any time off-centre of the bunch-overlapping region will exhibit a TOF difference for the tracks generated in the forward and backward regions, as shown on Fig. 3.4 (t_2–t_4, t_5–t_7, t_8–t_{10}). A mitigation factor of one order of magnitude necessitates a TOF precision of at least 30 ps [9].

Fig. 3.4 Schematics of bunch crossing and TOF in the forward and backward directions of particles generated by events created in different positions of the overlap region
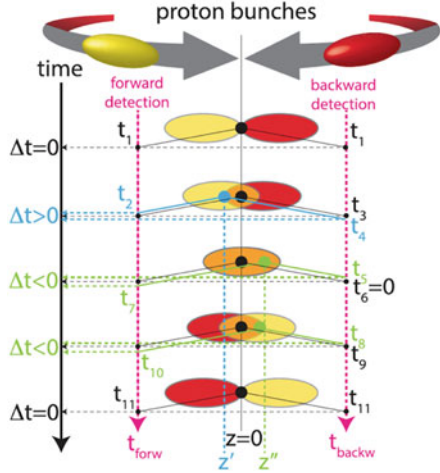
Excellent timing resolution is therefore needed. It can be shown [10] that it is related to the time density of the detected scintillation photons in the leading edge of the scintillation pulse, which is given by the following formula:

$$\sigma_t \approx \sqrt{\tau_r \tau_d \Big/ N_{pe}}$$

where τ_r and τ_d are the scintillator rise time and decay time respectively and N_{pe} is the number of photoelectrons produced in the photodetector, which is proportional to the light yield of the scintillator. A high light yield is therefore mandatory to minimize the photo-statistic fluctuation influencing the time jitter of the detector. An emission spectrum in the visible region is preferred as the quantum efficiency of the majority of photodetectors is higher and the light is generally less attenuated than in the UV region and hence more easily collected.

The energy resolution of the calorimeter is affected by all possible sources of non-uniformity. The light collection in a pointing geometry of tapered crystals introduces non-uniformity due to a focusing effect through the successive reflections of the light on the lateral faces, which depends on the refractive index of the crystal. Fluoride crystals and glasses, with low refractive index (around 1.5) have smaller non-uniformities (and therefore are easier to correct) than BGO (index 2.15) or PWO (index 2.3). The material can be intrinsically luminescent if it holds luminescent molecular complexes or ions, or is doped with a scintillating activator. Intrinsic scintillators are generally preferred, as it is easier to control the light yield uniformity in long crystals. On the other hand, a controlled distribution of the doping could help correcting for the non-uniformity caused by the light collection in a pointing geometry. Furthermore, the scintillation yield should be as independent as possible from temperature. Large temperature coefficients increase the complexity

of the detector design and of the software corrections, and temperature gradients between the front and back face of the crystals introduce non-uniformity affecting the resolution.

Finally, for large scintillator volumes cost considerations are of importance. The abundance of the raw materials, the facility to purify them against the most detrimental impurities to achieve good radiation hardness, a low temperature melting point to save on the energy cost, a high growing and mechanical processing yield are all parameters, which deserve particular attention.

3.1.3.2 Astrophysics and Space

Increasingly crystal-based calorimeters are embarked on satellites to study galactic and extra-galactic X- and γ-ray sources. This requires excellent energy resolution over a wide energy spectrum, typically from a few KeV to several TeV (see for instance Fig. 2.16 of ref. [11] for a list of different space missions with their respective energy range). One major aim of these measurements is the determination of the direction of the γ-ray source. Two classes of position sensitive devices have been developed in the last decades. These designs are using continuous scintillation crystal or pixilated detector geometries [12]. The required angular resolution is achieved with multilayer calorimeters or readout schemes to provide depth of interaction (DOI) information or using coded aperture masks.

The low orbit satellites are shielded by the earth magnetic field, relaxing therefore the requirement for radiation hardness of the scintillation material. Most of the scintillation materials can be used depending on the energy range of the detected γ-radiation. However, the payload is limiting the size of such detectors and not too dense materials are sometimes selected to reduce the weight.

In the interplanetary space the sun wind from charged particles strongly influences the detecting requirements of the scintillation materials. For these missions, high radiation hardness to ionizing radiation and low level of induced radioactivity are required. The same applies to detectors for planetary missions.

The general trend is to select high light yield, fast and not necessarily ultra-dense scintillators such as CsI or YAP. The very bright $LaBr_3$ is likely to find some applications in this domain because of its excellent low energy resolution (comparable to solid state detectors). BGO is very often used in veto counters for the rejection of Compton events.

3.1.3.3 Spectrometry of Low Energy γ-Quanta

This is probably the most important application domain for inorganic scintillators. The key requirement concerns energy resolution on the photopeak. It is therefore essential to maximize the photofraction and high Z materials are clearly preferred (see Sect. 3.1.1).

The energy resolution is driven by several factors and a detailed discussion is given in Sect. 3.1.1. However, two important parameters are playing an essential role. The first one is the light yield. One contribution to the energy resolution is the statistical fluctuation of the number of photoelectrons, n_{pe}, produced in the photodetector. Therefore a high light yield will reduce this statistical contribution like $(n_{pe})^{-1/2}$.

The second parameter concerns the deviations from the linearity of response at low energy. Most crystals exhibit a non-proportionality behaviour for energies below 100 keV. The relative light yield can show either relative increase with decreasing energy, as is the case for halide crystals, or a decrease, as for the majority of oxides and fluorides. Only few crystals have an almost linear response down to about 10 keV, such as $YAlO_3$ (YAP), $LuAlO_3$ (LuAP), $LuYAlO_3$ (LuYAP), $LaBr_3$. Given that the energy loss mechanisms—photoelectric, Compton scattering and pair production—are energy dependent, the total energy deposit in a crystal detector will be a mix of these contributions varying with energies. The non-linearity affects therefore the energy resolution, as is illustrated by the examples of Lutetium orthosilicate (LSO) and Lutetium Aluminium Perovskite (LuYAP). For the same detector volume, LuYAP achieves similar energy resolution (9%@511KeV) as LSO despite a three times lower light yield [13], as a result of a more linear response at low energy, as shown on Fig. 3.5.
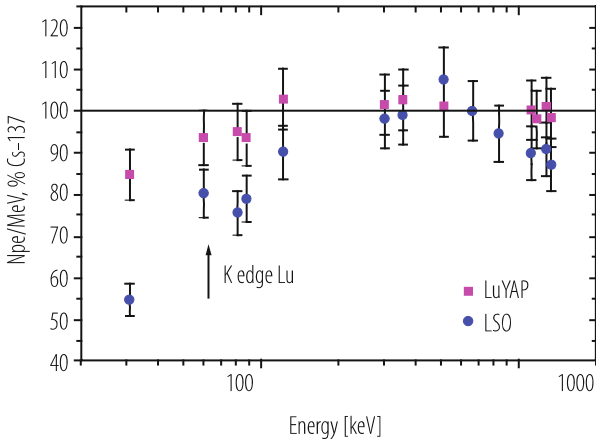
Fig. 3.5 Relative low energy response for LSO and LuYAP crystals, normalized to the ^{137}Cs energy peak (from ref [13])

3.1.3.4 Medical Imaging

Scintillators are widely used in medical imaging for X-ray radiology (digital radiography and CT scanners) and for emission tomography (PET and SPECT) with a market exceeding several hundred tons per year (see Sect. 20.1).

The choice of the scintillator for medical imaging devices is determined by the stopping power for the energy range of X and γ-rays to be considered, or more precisely the conversion efficiency. Materials with high Z and high density are favoured but the energy of the K-edge is also important as can be seen in Fig. 3.6. For low energy X-ray imaging (below 63 keV) the attenuation coefficient of Yttrium, Cesium and Iodine are quite high and crystals like YAP and CsI are good candidates for soft tissue X-ray imaging like mammography. Above the K-edge of Lu (63 keV) and Bismuth (90 keV) the situation is quite different and BGO and Lutetium based crystals are favored for bone, dental X-ray, ^{99}Tc (90 keV) SPECT and PET scanners (511 keV). Heavy scintillators have smaller thickness, reducing parallax errors in ring imagers and maintaining a good spatial resolution over the whole field of view (Sect. 7.1).

A high light yield is also mandatory for good energy resolution. Better energy resolution increases rejection of Compton events, improves the spatial resolution and the sensitivity. The sensitivity is a critical parameter as it determines the number of useful events per unit of injected dose. A higher sensitivity means a smaller injected dose or a better image contrast.

A short scintillation decay time reduces the dead time and therefore increases the maximum counting rate. In PET scanners for instance reducing the coincidence
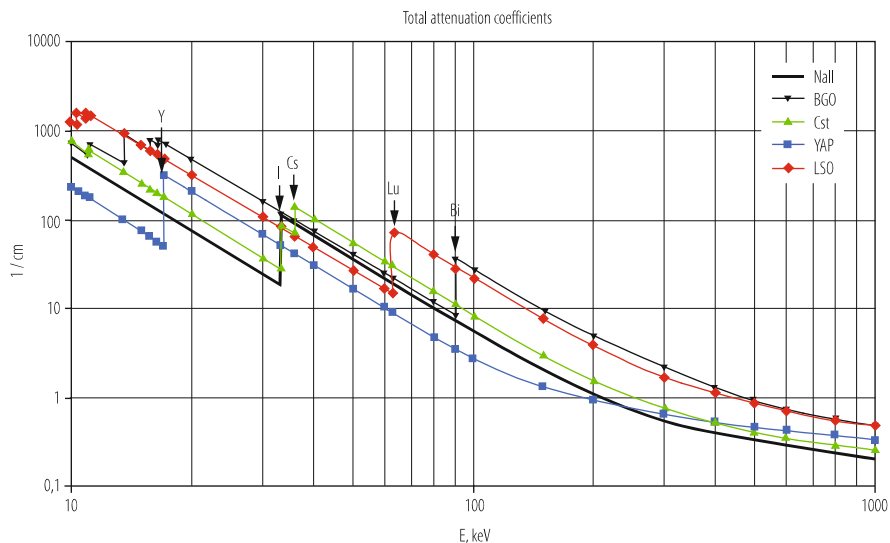
Fig. 3.6 Attenuation coefficients in several high Z materials
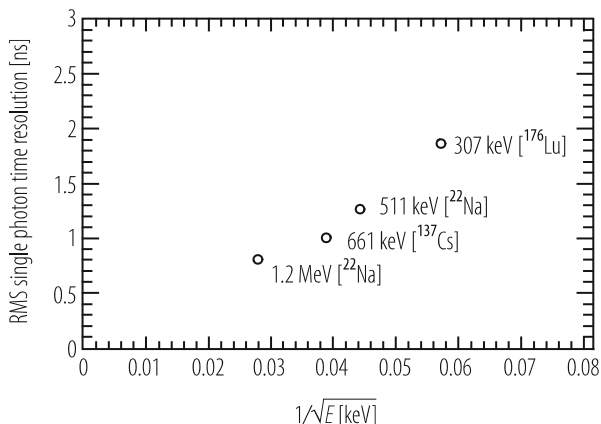
Fig. 3.7 Energy dependence of the timing resolution of a ClearPEM $2 \times 2 \times 20$ mm^3 LSO pixel coupled to an Hamamatsu avalanche photodiode (courtesy J. Varela)

window improves the signal to background ratio and increases the sensitivity and image contrast. Very fast scintillators open the way to scanners using the time-of-flight information, which helps reducing the background by selecting a narrow region of interest along the coincidence line. In the range of energies considered for medical imaging, the timing resolution is limited by the Poisson distribution of photons arrival time on the photodetector, even for bright scintillators like LSO. Figure 3.7 shows the $1/\sqrt{E}$ dependence of the timing resolution of a ClearPEM [14] detector head made of $2 \times 2 \times 20$ mm^3 LSO pixels coupled to a 32-channel Hamamatsu APD matrix, when excited by sources at different energies E.

Commercial PET scanners achieve about 500 ps FWHM coincidence time resolution (CTR) in the difference of detection time of the two 511 KeV gamma rays resulting from the positron annihilation. This allows a significant image quality improvement particularly for over-weighted patients. Ideally, one would like to achieve 100 ps FWHM CTR resolution, which would correspond to a centimetre resolution along the line of response (LOR) corresponding to the coincidence detection of the two gamma rays. It improves by an additional factor 5 the image signal-to-noise ratio. Thus a TOF-PET system with 100 ps CTR can either give a five times shorter examination time of the patient or a five times lower radiation dose at constant image quality.

As mentioned in Sect. 3.1.2.2, in first approximation (assuming single photon detection) the CTR for a scintillators with a scintillator rise time τ_r and a decay time τ_d, is given by:

$$CTR \propto \sqrt{\frac{\tau_r \tau_d}{N_{phe}}}$$

where N_{phe} is the number of photoelectrons readout from the crystal. Clearly, there is a premium for a high photon rate in the leading edge of the scintillation pulse, a high light yield as well as a short rise and decay times for improving the CTR.

3.1.3.5 Safety Systems and Homeland Security

Scintillators are used in three main types of equipment related to safety and homeland security: express control of luggage and passengers, search for explosive materials and remote detection of fissile materials.

Luggage inspection requires the highest possible throughput to quickly identify a suspect luggage in a few cubic meter large container moving across the inspection device. The spatial resolution is determined by the need to quickly localize and identify the suspect object in a large container. Fast scintillation kinetics with no afterglow is therefore the most important parameter.

For the remote detection of explosives the most attractive methods are based on the detection of natural or induced characteristic neutron and γ-rays under activation by a neutron source, either with fast neutrons from the ^{252}Cf radioisotope or fast-thermal neutrons from a pulsed electronic neutron generator. Neutrons initiate nuclear reactions in some elements, some of them producing characteristic γ-rays. Plastic explosives for instance are generally rich in nitrogen. The nitrogen (n,γ) reaction has a cross section of 75 mb and produces a characteristic γ-ray of 10.83 MeV.

For such applications, the most important scintillation crystal parameters are: high stopping power to improve the detector sensitivity; high light yield to improve the detector energy selectivity; fast scintillation decay time to allow time-of-flight analysis with pulsed neutron generators to increase the signal to noise ratio. Good stability of the scintillator parameters under ionizing and neutron irradiation allows the use of strong activation sources for a better sensitivity.

Remote detection and fissile materials warhead inspection has been for a long time restricted to the detection of neutrons, as the γ-channel would have easily revealed secret characteristics of the nuclear device. This has changed recently and opens new possibilities to detect the radiation emitted by Nuclear Explosive Devices (NED) based on enriched uranium or plutonium. The most useful energy range to detect fissile material is $E_\gamma \geq 3$ MeV because of (1) the absence in this range of natural radioactive sources and therefore an acceptable signal to background ratio; (2) the high penetration power of these energetic γ-quanta making the deliberate concealment of the intrinsic NED radiation more difficult.

Here, the most important parameters are sensitivity to allow detection at large distance (at least several meters) and good background rejection. High stopping power (and therefore high density) is mandatory. However, the crystals should be made from materials with very low natural radioactivity, which restricts the choice of heavy materials to the ones with no unstable isotopes. As the counting rates are usually low, there is no need for ultra-fast scintillators. A phoswich geometry based on two different crystals on top of each other can be an attractive solution for

improved low energy background rejection. A first thin scintillator layer detects (and rejects) the low energy background activity, whereas a thicker layer on the back will be mainly sensitive to the 3–10 MeV range of interest. The two scintillators must have different emission wavelength and/or decay time for a good identification of the hit source.

3.1.4 Organic Material, Glass and Condensed Gases

There is a particular class of scintillators, which does not require a regular lattice to produce scintillation light when excited by ionizing radiation. These are organic solid and liquid materials, condensed gases as well as scintillating glasses. A common feature of all these materials is that scintillation (also called fluorescence in this case) results from a direct excitation of a molecule and does not involve the transport of the excitation energy through the material. As the molecule is directly excited and the coupling with the host material is minimal, the fluorescence decay time is solely determined by the quantum numbers of the excited and ground states. If properly chosen the molecule will emit between two singlet states giving rise to a fast emission (usually not more than a few ns).

Different material combinations can be engineered, in particular in plastic scintillators, to meet specific requirements. The most popular one concerns wavelength shifters. Binary or even ternary solutions of different fluors can be dissolved in a plastic base containing aromatic molecules. After excitation by ionizing radiation, these aromatic rings will relax the stored energy by emitting UV photons. Properly chosen additional fluors can absorb these photons and reemit them at longer wavelength, e.g. to better match the quantum efficiency of a photodetector. As there are only energy transfer and no charge transfer mechanisms involved, the whole process is very fast.

Plastic scintillators can be easily machined in any shape, including in the form of fibres, one important advantage. However, these materials are intrinsically light (density around 1–1.2 g/cm^3) and therefore are not suitable for homogeneous calorimetry. They find a number of applications in sampling calorimetry and tracking. More information can be found in ref. [15].

3.2 Scintillation and Quenching Mechanisms in Inorganic Scintillators

### 3.2.1 The Five Steps in Scintillation Process

In contrast to luminescence (such as in lasers), where the excitation source is tuned to the energy levels of the luminescent centres, scintillation is the result of a

complex chain of processes, each of them characterized by a specific time constant and efficiency factors [16]. This is summarized in Fig. 3.8, where the valence and conduction bands of an insulator with a bandgap width E_g (forbidden band) are represented. The upper level core band (energy E_c and bandwidth ΔE_c) is also shown.

The sequence of processes is shown as a function of time and can be qualitatively divided into five main phases:

- The first one is the energy conversion phase and the subsequent production of primary excitations by interaction of ionizing particles with the material. For an incident particle energy in the keV range or higher, the excitations are essentially deep holes h created in inner core bands and hot electrons e in the conduction band. Subsequently, on a very short time scale (10^{-16}–10^{-14} s), a large number of secondary electronic excitations are produced through inelastic electron-electron scattering and Auger processes with creation of electrons in the conduction band and holes in core and valence bands. At the end of this stage, the multiplication of excitations stops. All electrons in the conduction band have an energy smaller than $2E_g$ (e-e scattering threshold) and all holes occupy the valence band if there is no core band lying above the Auger process threshold (general case).
- The second stage is the thermalization of electronic excitations through a phonon coupling mechanism with the crystal lattice, leading to low kinetic energy electrons in the bottom of the conduction band and of holes in the top of the valence band. This thermalization phase takes place in the sub-picosecond range, typically between 10^{-14} and 10^{-12} s.
- The next stage, between 10^{-12} and 10^{-10} s, is characterized by the localization of the excitations through their interaction with stable defects and impurities of the material. For example, electrons and holes can be captured by different traps or self-trapped in the crystal lattice. Excitons, self-trapped excitons, self-trapped holes (V_K centers) can be formed with emission of phonons. Localization of excitations can be sometimes accompanied by displacements of atoms (defect creation, photo-stimulated desorption).
- The transfer of excitations to the luminescent centres through the sequential capture of charge carriers or different energy transfer mechanisms takes place during the following 10^{-10} and 10^{-8} s.
- Finally, the radiative relaxation of the excited luminescent enters produces the light signal with an efficiency and time structure, which is given by the quantum selection rules of the transition. Parity allowed transitions with more than 3 eV energy gaps are generally preferred as they give rise to fast luminescence. However, smaller energy gaps (2–3 eV) are likely to favour higher light yield, as discussed in Sect. 3.1.2.2.

The scheme depicted in Fig. 3.8 describes the scintillation mechanisms in the case of ionic crystals with simple energy structures. However, important groups of scintillators exhibit a more complicated band structure.
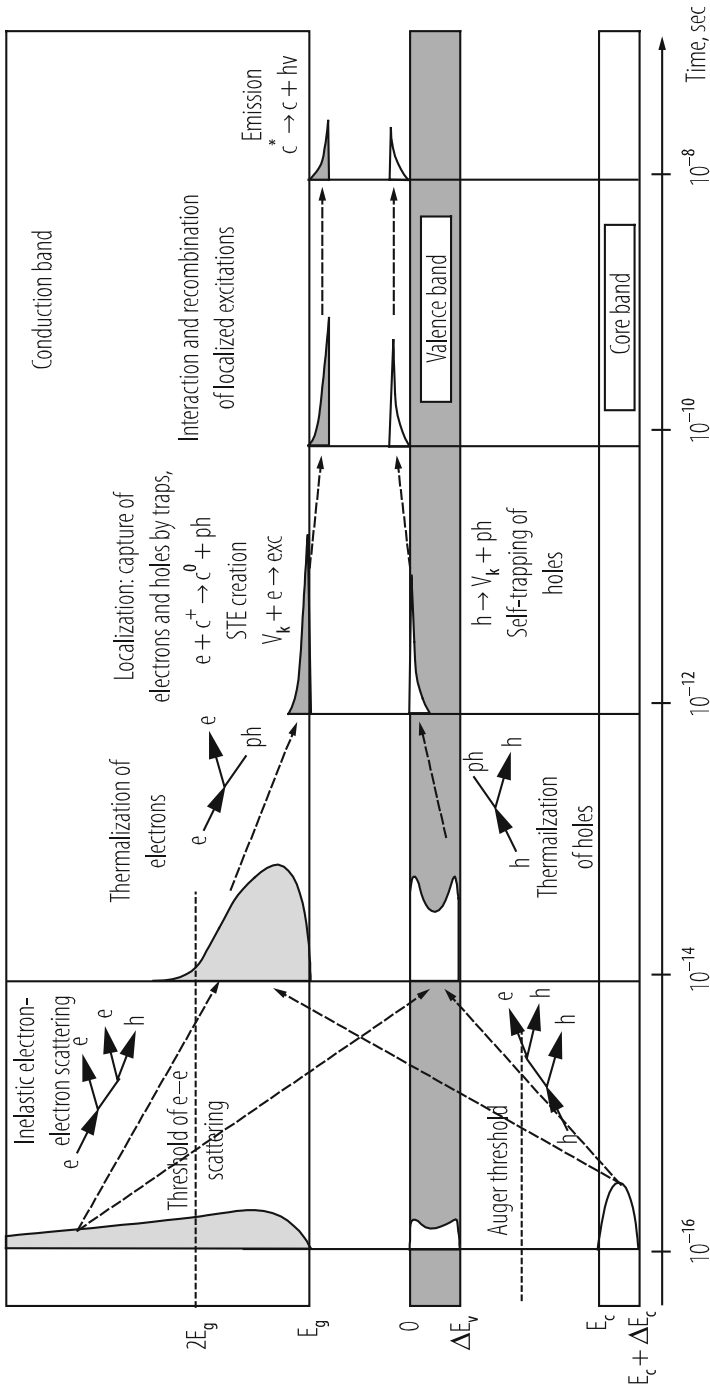
Fig. 3.8 Relaxation scheme for electronic excitations in an insulator: e, electrons; h, holes; ph, phonons; hν, photons; V_k, self-trapped holes; STE, self-trapped excitons; c^n, ionic centers with charge n. Density of states is represented by grey and white areas for electrons and holes respectively (courtesy A. Vasiliev)

One such case are so-called cross-luminescent materials, of which one well-known example is Barium Fluoride (BaF_2). Such systems are characterized by a specific configuration of the energy bands, such that the width of the forbidden gap (between the valence and conduction bands) is larger than the energy gap between the uppermost core band (5pBa in the case of BaF_2) and the bottom of the valence band. When a hole produced in this core band recombines with an electron of the valence band there is not enough energy available to eject an Auger electron from the valence to the conduction band. The core-valence transition can therefore only be radiative giving rise to a scintillation in the UV, which is usually very fast (sub-nanosecond).

3.2.2 Scintillation Efficiency

The overall scintillation efficiency η is generally given by the product of three terms:

$$\eta = \beta \cdot S \cdot Q \tag{3.10}$$

where β represents the conversion efficiency for the production of electron-hole pairs, S the excitation transport efficiency, including thermalization of electric carriers, localization and transfer to the luminescent centre, and Q is the quantum efficiency of the radiative transition of the luminescent centre. If we consider, as discussed in Sect. 3.1.2.2, the number of 140,000 ph/MeV as an upper limit for the scintillation yield of an ideal scintillator with an emission peak around 600 nm the maximum scintillation efficiency is less than 30%. In reality, for the majority of existing scintillators it is less than 5%, mostly because of important losses during the thermalization and transport process.

At the end of the first phase of inelastic scattering the holes and electrons have reached an energy below the Auger and ionization thresholds respectively. Their thermalization to the top of the valence band for holes and to the bottom of the conduction band for electrons can only take place by heat dissipation through coupling to the phonon modes of the lattice. This is an unavoidable part of energy loss for the scintillation process. The energy gap between these two thresholds being of the order of $2.3E_g$ for ionic crystals one concludes that an ideal scintillator cannot convert more than 43% of the absorbed energy into light.

Another important loss is related to the transfer of the excitations to the luminescent centres. A frequent channel of excitation for acceptors is a charge transfer process with a sequential capture of charge carriers. In Ce^{3+}-doped crystals, the hole is first captured with its capture probability strongly depending on the position of the Ce^{3+} ground level (4f) in the forbidden band gap. In cerium-doped oxides and halides, this level is usually lying very low in the gap close to the top of the valence band, and these systems can lead to very efficient scintillation (LSO, LuAP, $LaCl_3$, etc.). On the other hand, Ce^{3+}-doped fluoride crystals cannot exhibit

very high light yield because the Ce^{3+} 4f is lying around 3–4 eV above the valence band, which strongly reduces the hole capture probability.

It is also important to avoid the delocalization of electrons from the activator excited state to the conduction band. This is achieved if the energy gap ΔE between the radiating level of the doping ion and the bottom of the conduction band is large enough. If $\Delta E \gg kT$, or the radiative decay $\tau_\gamma \ll \tau_d$, where the delocalization time $\tau_d \approx (1/S)\exp(-\Delta E /kT)$, with S—the frequency factor, k—the Boltzman constant, and T—the temperature, the scintillation yield is not strongly dependent on the temperature. In the reverse case one can expect a reduction of the scintillation yield when the temperature increases (temperature quenching). Similarly, when the ground state is located in or very close to the valence band, the hole is weakly trapped and can be easily delocalized to the valence band.

Besides these different processes, a number of competing channels can limit the probability of charge carrier capture by the luminescent centres. Impurities or ions in the lattice can act as specific killer ions and compete with active ions for the capture of charge carriers and/or interact with them, inducing severe limitations in scintillation efficiency. For example, in cerium-doped crystals the presence of ions or molecular groups with two or more stable valence states is generally to be avoided. This is due to the fact that cerium has two stable valence states, Ce^{3+} and Ce^{4+}, but Ce^{3+} only gives rise to luminescence. If a possibility exists for Ce^{3+} to transfer one electron to these killers it will transform into Ce^{4+} and no longer scintillate. This is the case for Ce-doped tungstates and vanadates, which do not exhibit cerium scintillation because of such Ce-W and Ce-V interactions. For the same reason the good electron acceptor Yb^{3+} severely quenches the Ce^{3+} scintillation.

Self-trapping is also a very frequent source of efficiency loss in insulating materials. Indeed, some of the electrons and holes can be trapped by impurity or crystal defect related acceptors and cannot excite directly luminescent centres through sequential capture. If the trap is very shallow it will quickly release the charge carriers and will slightly delay scintillation. However, in deep traps strong quenching of the fast luminescence components is observed. Very long components in the fluorescence decay appear when the temperature is raised to the point, where trapped electrons can be released by thermal energy (glow peaks).

The interaction between closely spaced electronic excitations (in a few nanometre range) may lead to luminescence quenching, also-called local density-induced quenching. For electronic excitations created through the different mechanisms of photon absorption, the probability to produce excitations at such short distances is very low if the excitation source has a limited intensity. On the contrary, secondary electronic excitations created by inelastic scattering of photoelectrons or Auger decay of core holes can be quite closely spaced. In these clusters of high local e and h density, the interaction between excitations can modify their localization and can even create defects in crystals. In addition, these clusters can excite closely spaced luminescent centres, which can interact with each-others, giving rise to faster and

Fig. 3.9 The configurational coordinate diagram. The energy E is plotted versus the coordinate Q (configurational coordinate in the lattice). The ground state g and one excited state e are represented by potential curves with offset ΔQ. Absorption and emission transitions are indicated
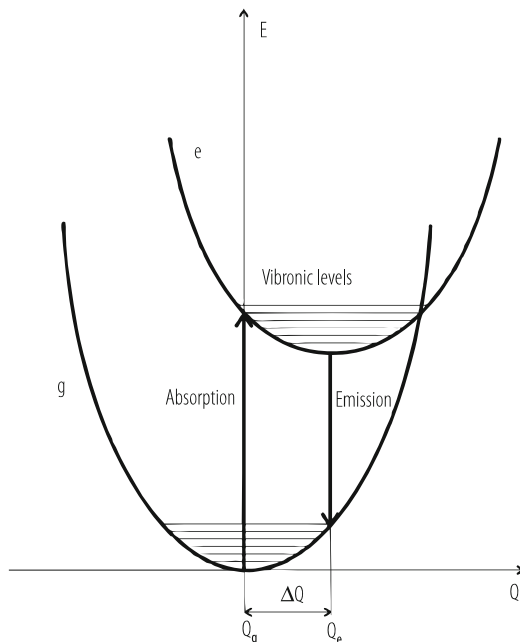
non-exponential decay time and total or partial luminescence quenching. The first evidence of such effect was observed in CeF$_3$ [17].

Another type of thermal quenching can occur related to electron-phonon coupling. The different electronic configuration of the ground and excited states of the activator generally induces an exchange of phonons and the relaxation of the position of the activator ion when it is excited. As a result, the emission transition from the relaxed excited state is shifted towards lower energy than the absorption transition. This is the well-known Stokes shift illustrated in Fig. 3.9. The Stokes shift is a measure of the interaction between the emitting centre and the vibrating lattice. The stronger the electron-phonon coupling the larger the Stokes shift. For weak coupling, the potential curves are not significantly shifted and the emission spectra show narrow lines (case of f-f transitions of rare earth ions). In the case of intermediate coupling for which the parabolas are weakly shifted, vibronic spectra of broad emission lines are observed reflecting the progression in stretching vibration of the luminescent ion (case of uranyl pseudo-molecules in oxides, like UO$_2{}^{2+}$).

In the case of strong coupling (shown in Fig. 3.8) the relaxed excited state may decay non-radiatively to the ground state if the temperature is high enough to allow the excitation to reach the crossing of the two parabolas.

In practice, the relevant parameter is the light yield efficiency Y, which is the product of the scintillation yield η by the light transport and collection efficiency η_{col} to the photodetector. A number of parameters influence η_{col}: the crystal shape, its optical transparency to the scintillation wavelength, the presence of scatters and

different optical defects in the bulk of the crystal, the surface state and wrapping conditions of the faces of the crystal, the coupling face to the photodetector, the surface matching between the coupling face and the photodetector, the crystal index of refraction. Heavy scintillators generally have a high index of refraction (larger than 2 in many cases) and the light collection efficiency is limited to 10–30% for the majority of existing detectors. New approaches based on nanostructured surfaces, in particular photonic crystals, are presently being explored [18]. Significant light extraction gains of more than 50% have been obtained as well as a strong reduction of the photon transit time spread in the crystal associated to the higher extraction probability of the photons at their first hit on the coupling face to the photodetector (reduction of multiple bouncing) [19].

The fact that some self-activated scintillators, like $PbWO_4$, exhibit fast room temperature scintillation in the ns-range is only the consequence of a luminescence quenching mechanism competing with the radiative relaxation of the excitation. In this case the decay is non-exponential, which is a common signature of temperature quenched scintillators.

3.2.3 Response Linearity and Energy Resolution

The ultimate energy resolution (FWHM) of a perfect scintillator based detector is given by the well-known Poisson law:

$$R_{\lim} = 2.35 \sqrt{\frac{1 + v(PD)}{N_{pe}}} \tag{3.11}$$

where $v(PD)$ is the variance of the photodetector gain and N_{pe} is the number of photoelectrons emitted by the photodetector. As the number of photoelectrons is proportional to the number of photons N_{ph} produced by the scintillator, the resolution should be driven by the photostatistics of the scintillator light production. However, several other factors contribute to the practical resolution R:

$$R^2 = R_{\lim}^2 + R_{inh}^2 + R_{tr}^2 + R_{np}^2 \tag{3.12}$$

where R_{inh} reflects homogeneities of the crystal, inducing local variations of the scintillations efficiency, R_{tr} is related to the light transport and collection by the photodetector and R_{np} is a factor of non-proportionality, which accounts for the fact that for some scintillators, the number of emitted photons is not strictly proportional to the incident energy.

Non-linear response has been first reported for NaI(Tl) and CsI(Tl); the response per unit deposited energy decreases continuously from X- and γ-rays to electrons, protons, α particles, and fission fragments. Moreover, this trend is strongly correlated with the ionization density dE/dx [20]. In other words, the response of

a scintillator depends not only on the total amount of energy but also on the mechanisms of the energy deposit. There is common agreement that this is related to the saturation of response of the luminescent centres in the presence of a high density of charge carriers. This is parameterized by Birks law, which postulates a non-radiative relaxation of excitons interacting with each others in the case of high ionization density:

$$N_{ph}\left(\frac{dE}{dx}\right) = \frac{N_{ph}^0}{1 + a_B \frac{dE}{dx}} \tag{3.13}$$

where N°_{ph} is the light yield in the absence of saturation, N_{ph} is the actual light yield and a_B is the Birks parameter.

When combining the $1/\beta^2$ ionization density increase for low energy particles of decreasing velocity β (Bethe Bloch formula) with the Birks saturation law one obtains the typical scintillator non-linear response at low energy as illustrated on Fig. 3.10 in the case of NaI(Tl) [21].

It remains, however, to be explained why some scintillators are more affected by this saturation effect than others.

Each of the steps of the conversion process described in the previous section can be characterized by a certain degree of non-linearity. It seems, however, that last stages of thermalization and capture are the most affected by non-linear phenomena. Indeed, as long as the kinetic energy of electrons and holes is large relative to the bandgap E_g the excess energy will be used to produce secondary e-h pairs and this energy conversion process is intrinsically linear. On the other hand the stability of the thermalized excitons in its crystallographic environment is very much dependant on the energy band structure of the material as well as on the density of luminescent centres or defects. This stability is related to the correlation distance between the electron and hole, which is energy and temperature dependant.
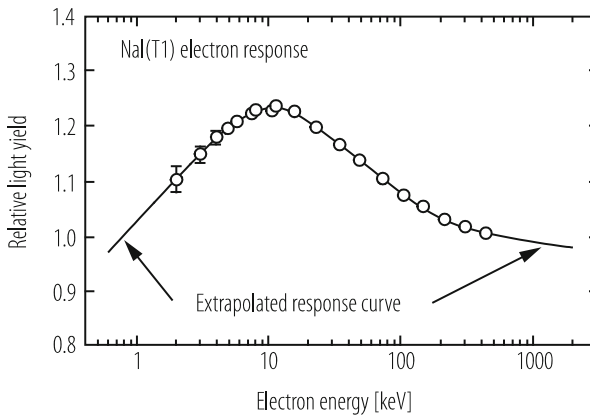
Fig. 3.10 Measured electron response for NaI(Tl) scintillator (from ref [21])
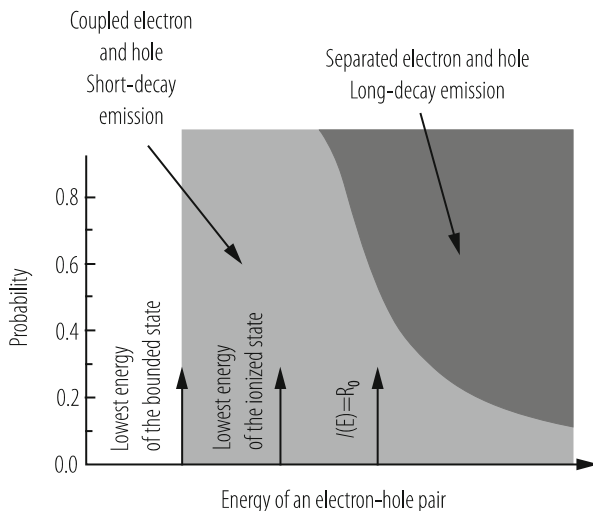
Fig. 3.11 Probability of binding or separation of an e-h pair as a function of energy (courtesy A. Vasiliev)

Two competing recombination processes can take place, both being intrinsically non-linear with energy as shown on Fig. 3.11, and inducing therefore a non-linear energy response of the scintillator. The first one is the self-trapping of the exciton in the vicinity of a luminescent centre which decreases rapidly with the e-h pair energy. The second one is the direct capture of the separate electron and/or hole by defects or luminescent centres and increases with the kinetic energy of the electron and hole.

The energy threshold between these two mechanisms is related to the correlation distance R_0 between the electron and hole, which is temperature dependant. As a result, the energy dependence of the scintillator response to thermalized e-h pars is strongly non-linear as shown on Fig. 3.10, which also shows the influence of the defects (crystal quality) on the excitation transfer efficiency to the luminescent centres.

The quantitative link between the low energy non-linearity of the scintillator response and the deviation of its energy resolution from the predicted counting statistics is far from being fully understood. It has however its seed in the fact that for the same total amount of deposited energy both photons and electrons release this energy in a number of quanta over a large energy range and that the light response for each of these quanta has different proportionality constants as a function of energy. The event-to-event variation of this cascade process induces a spread in the energy response, which deteriorates the energy resolution.

This is obvious in the case of Compton scattering. In a detector of a finite size, the events in the photopeak result from the sum of true photoelectric events and of events having undergone single or multiple Compton scattering interactions all

contained in the detector block. The total energy deposited in the detector block is the same whether it results from a single or multiple interactions. The light response may however differ due to the non-linear response of the scintillator. As a result, the event-to-event statistical variation of the energy deposition mechanism induces a broadening of the resolution.

As pointed out in ref. [22] one would expect an improvement of the resolution by reducing the detector size, as the fraction of fully contained Compton events decreases and consequently the proportion of true photoelectric events increases. This is actually not the case, because photoelectric events may result at the atomic scale from a complex cascade mechanism. Indeed, the photoelectric interaction of an X- or γ-ray produces a mono-energetic electron from one of the inner shells of the atoms of the absorber. However, this electron can be ejected not only from the K shell but also from a L or even a M shell (although the cross-section rapidly decreases for higher core levels) of the different atoms of the crystal. In the sequence of photon detection, recoil electrons with different energies are produced, each carrying the incident photon energy minus the binding energy of the shell, from which it has been ejected. Moreover, the deep hole produced in the inner shell will be filled by an electron from outer shells, which in turn will be replaced by electrons rom even lower bound shells through a cascade of relaxation events, each of them producing an X-Ray or an Auger electron converting in the crystal following the same mechanisms. Figure 3.12 depicts a part of this cascade process for LSO crystals, commonly used in medical imaging cameras.

Finally, the recoil electrons, as well as all charged particles detected in a scintillator, slow down through a sequence of energy transfers to the absorber with a progressively increasing ionization density.

The energy resolution of calorimeters used in high or medium energy physics is generally parametrized as a function of energy according to the following formula:

$$\frac{\sigma(E)}{E} = \frac{a}{\sqrt{E}} \oplus \frac{b}{E} \oplus c \tag{3.14}$$

where a is the statistical term, b the noise term and c a constant term, which takes into account all the systematics (intercalibration error, temperature effects, light yield non-uniformity in the crystal, shower leakage, etc.).

At high energy, the constant term is predominant and it requires a challenging engineering effort to reach the sub-percent level for large detector systems with tens of thousands of channels. This has been achieved for the LEP L3 BGO calorimeter (with 12,000 crystals) with a high energy resolution of 1% and in the LHC CMS PWO calorimeter (77,000 crystals) with a constant term of better than 0.5%.

At lower energy, the electronic noise plays an increasing role. The noise contribution, which is energy independent, contributes therefore to the *relative* energy resolution (3.14) as 1/E.

An interesting example is given in Fig. 3.13 for two heavy Lutetium based crystals popular for medical imaging devices, LSO and LuYAP. In spite of a light
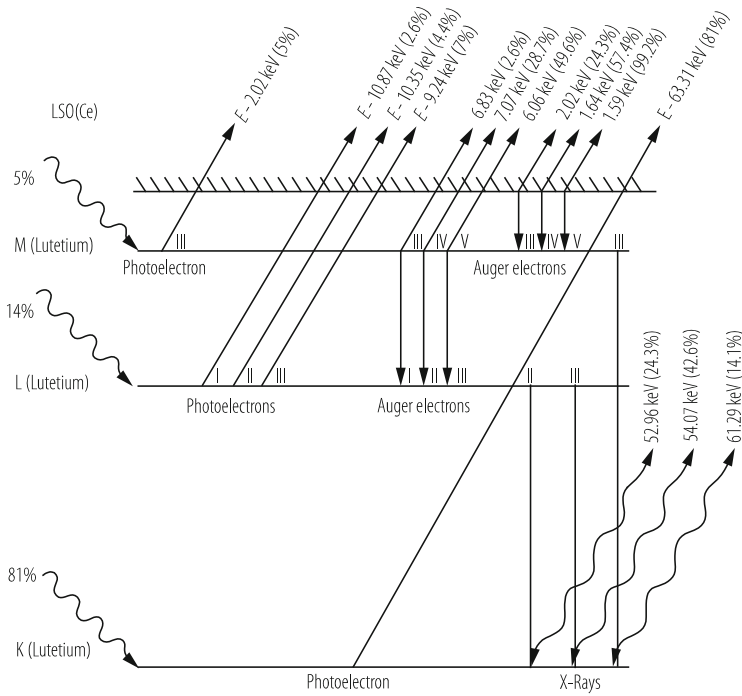
Fig. 3.12 Electron cascade following photoelectric absorption in LSO Crystal. *E* refers to the photoelectrically absorbed photon energy (ref. [22])

yield nearly three times lower LuYAP achieves a comparable energy resolution than LSO because of a much more linear behavior at low energy (see Fig. 3.4).

3.2.4 Scintillation Kinetics and Ultrafast Emission Mechanisms

Achieving ultimate time resolution on scintillator-based detectors requires a parallel effort on the light production mechanisms, light transport optimization to reduce the travel time spread of the photons on their way to the photodetector, on the photoconversion system as well as on the readout electronics.

As shown in Sect. 3.2.1 the radiative transition on the activator ion or on the intrinsic luminescent center only takes place after a complex relaxation mechanism of the primary electron-hole pairs that can last several nanoseconds. In this process large statistical fluctuations are therefore induced for the generation of the first scintillation photons, which influence the observed rise time. This presents an intrinsic limit to the achievable time resolution in a scintillator. It is related to the
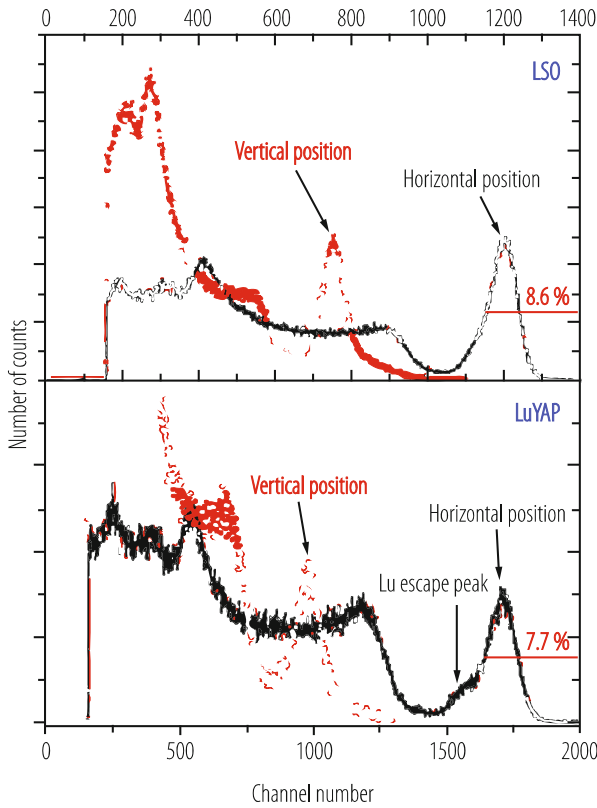
Fig. 3.13 Energy resolution for ^{137}Cs photons obtained with $2 \times 2 \times 10$ mm^3 Ce doped LSO and LuYAP crystals measured in horizontal and vertical position. The electronic gain for LuYAP is three times higher to compensate for the lower light yield (6000 pe/MeV and 2000 pe/MeV for LSO and LuYAP, respectively, in horizontal position)

time fluctuations in the relaxation process that can be estimated to be of the order of 100 ps.

For sub-100 ps time resolution mechanisms involving the production of prompt photons need to be considered. Cherenkov emission and cross-luminescent materials can offer a solution. However, the number of Cherenkov photons from the recoil electrons resulting from a 511 KeV γ conversion is very small, of the order of 20 photons in crystals like LSO, LuAP and GSO. Moreover, these photons are preferentially emitted in the UV part of the spectrum, where the optical transmittance and the photodetector quantum efficiency are generally low. The same applies for cross-luminescent materials characterized by a reasonably fast emission (600 ps for BaF$_2$) which emit in the 100–250 nm spectral range. However, some transient phenomena in the relaxation process that can be possibly exploited for the generation of prompt photons. From this point of view, an interesting phase of the relaxation mechanism is the thermalization step when the hot electrons and
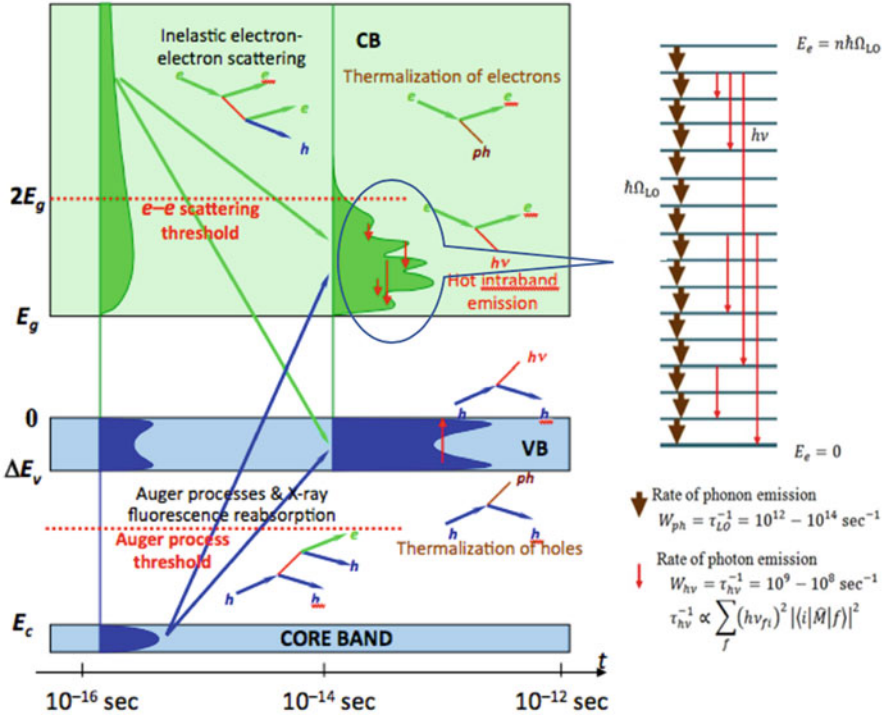
Fig. 3.14 Schematic description of the hot intraband luminescence, showing the competition of radiative and non-radiative (phonon-assisted) decay channels in the case of a non-uniform density of states in the conduction band. From Ref [23]

holes have passed the ionization threshold. The coupling to acoustic and optical phonons in the lattice is the source of hot intraband luminescence (HIBL) that could be exploited to obtain a time tag for the interaction of ionizing radiation with a precision in the picosecond range [23, 24]. This emission is rather weak but extremely fast (sub-ps) and is characterized by a flat spectrum in the visible for the electron-induced HIBL in the conduction band with an onset in the near infrared attributed to the hole HIBL in the valence band. Work is ongoing to engineer scintillators with a non-uniform density of states in the conduction and/or the valence band which may result in a more intense HIBL emission (Fig. 3.14). Already a few hundred prompt photons would suffice to significantly improve the time resolution of scintillators like LSO in the low energy (MeV) regime.

Hetero-structures based on a combination of standard scintillators (such as LSO or LYSO) and nanocrystals may be another way to produce prompt photons. Nanocrystals have gained considerable attention over the last two decades because of their excellent fluorescence properties. In such systems quantum confinement offers very attractive properties, among which a very high quantum efficiency and ultrafast decay time. Moreover, they have a broadband absorption and narrow emis-

sion, enhanced stability compared to organic dyes, and the fluorescence is tunable from the UV to the near-infrared spectral range (300–3000 nm) by nanocrystal size and material composition.

A novel route towards the realization of ultrafast timing resolution is possible with the use of colloidal CdSe nanosheets (CQwells) [24], a new class of two-dimensional materials. CQwells are solution-processed analogs to epitaxial quantum wells (Qwells). However, being synthesized in solution, they can be deposited on any substrate with arbitrary geometrical configuration. Further, a large dielectric mismatch between the inorganic CdSe CQwells and the surrounding organic environment results in much stronger quantum confinement than in epitaxial Qwells. This mismatch combined with very little dielectric screening due to the 1.5 nm CQwell thickness results in strongly enhanced exciton and biexciton binding energies of 132 and 30 meV, respectively, making both populations stable at room temperature.

The strong electron and hole confinement in one dimension and free motion in the plane has several important consequences, including strict momentum conservations rules (in contrast to quantum dots) and a giant oscillator strength transition. Momentum conservation in CQwells limits the available states for Auger transitions, reducing the recombination rate of this nonradiative channel. In addition to the enhanced exciton and biexciton binding energies, a giant oscillator transition results in radiative lifetimes that are significantly shorter than in bulk CdSe (~400 and ~100 ps, respectively). All of these properties contribute to the ultralow threshold stimulated emission (or superluminescence) with sub-ps decay time that has been observed with these CQwells (Fig. 3.15). Such systems could find
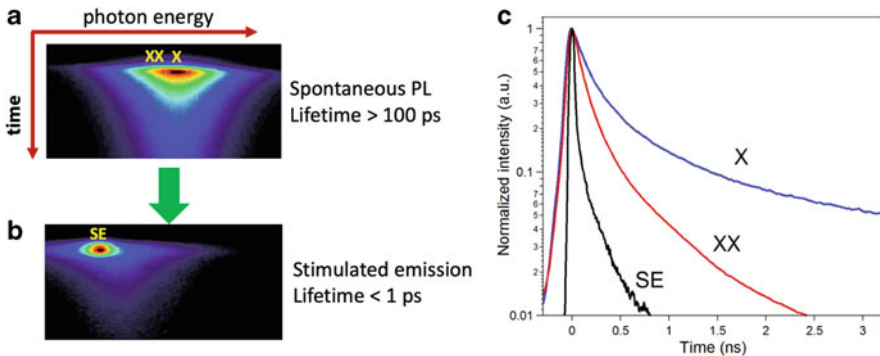
Fig. 3.15 Time-resolved spectral decay under femtosecond excitation (**a**) Streak image showing the spectral decay of exciton (X) and biexciton (XX) emission from CdSe CQwells. (**b**) Stimulated emission at an ultralow excitation fluence of $F_0 = 6\,\mu J/cm^2$, with characteristic spectral narrowing and lifetime shortening. From Ref [24]

interesting applications in ultrafast X-Ray imaging as well as providing a fast time tag in γ imaging if used in hetero-structures in combination with dense scintillators like LSO with a structuration dimension of the order of the recoil electron range, as suggested in Ref [25].

3.3   Role of Defects on Scintillation Properties and on Radiation Damage in Inorganic Scintillators

3.3.1   Structural Defects in a Crystal

The properties of a scintillator strongly depend on the structural quality of the crystal lattice. The presence of defects influences all stages of the scintillation process. They play also an important role in the light transport to the photodetector, as well as in the generation of optically active defects under radiation exposure. They continuously exchange charge carriers and phonons with the crystal lattice and are therefore in thermodynamic equilibrium with the medium. This can have a number of consequences such as reduced or enhanced scintillation efficiency if the charge carriers are channelled through these defects to non-radiative or radiative traps respectively, modification of the scintillation kinetics, afterglow, creation of perturbed emission centres, self-absorption, emission wavelength shift, radiation damage, radiation damage recovery. Depending on their size and physical nature, one can distinguish two main classes of structural defects, namely point size defects and impurities. Larger scale defects such as dislocations, twins, voids and other macroscopic defects also exist. They will not be described here, as their influence on the crystal properties is usually limited to the mechanical ruggedness and to a small extent to the optical homogeneity.

3.3.1.1   Point Size Defects

A perfect crystal is a virtual object that can only exist at absolute zero temperature. At higher temperature, a thermodynamic equilibrium is obtained by exchange of energy quanta (in the form of phonons) between the environment and the crystal lattice. Moreover, the finite dimensions of the crystal imposes conditions on the surface to compensate the electrostatic field unbalance for the atoms at the interface. This requires some level of plasticity of the lattice, which is generally achieved by a certain concentration of cation and anion vacancies. Thermodynamics imposes a relatively low concentration of such defects at room temperature, typically of the order of 10^{12} cm^{-3}. For comparison, the atomic density of the majority of known heavy scintillators is about 10^{23} cm^{-3}. In practise, the concentration of vacancies is determined by the crystal growth technology. The melt is a mixture of several chemical components, each of them with a different melting temperature

and vapour pressure, which leads to segregational evaporation of some components. Furthermore, close-to-surface vacancies can be partially compensated by absorption of ions or radicals from the surrounding atmosphere. Typically the concentration of such defects is at the level of 10^{18} cm^{-3} (10 ppm atomic) or even more. At such concentration, some collective effects can take place, leading to more complex molecular or cluster defects. Another typical point defect results from the displacement of an ion of the lattice to an interstitial position. The electrically neutral system behaves as a dipole and is called a Frenkel defect. In the case of Lead Tungstate an oxygen-based Frenkel defect is responsible for an absorption band at 360 nm and for an increased susceptibility to radiation damage.

3.3.1.2   Impurities

Impurities are ions of different nature than the constituents of the crystal lattice. They are generally introduced from imperfectly purified raw materials or by contamination, for instance from the crucible material, during the crystal growth process. Doping ions acting as luminescence activators, such as Ce^{3+} in LSO, LuAP and many other fast scintillators, can be considered as impurities with a positive role. Ions from the lattice, but in a different valence state than required by the electric charge balance, are another type of impurity. As an example, Ce^{4+} has been considered by some authors as a possible scintillation quencher in CeF_3 crystals. Two important parameters influence the way impurities can be introduced in a crystal: their electric charge and their ionic radius. If the ionic radius is close to the one of ions from the lattice, impurities can easily replace these ions, producing only a small distortion of the lattice. Isovalent ions will then easily produce a solid solution as is the case for LYSO or LuYAP when Y^{3+} ions substitute Lu^{3+} in LSO and LuAP crystals, producing locally a mixed compound of LSO-YSO and LuAP-YAP, respectively. If heterovalent impurities are introduced in the crystal their charge excess or deficit must be compensated by other impurities or by lattice ion vacancies. This mechanism can be used to suppress the detrimental role of some defects, which cannot be eliminated. A good example are the lead vacancies in PWO, which are efficient hole traps responsible for radiation damage and which can be compensated by substituting trivalent ions such as Y^{3+} or La^{3+} to neighbouring Pb^{2+} ions in the lattice.

Impurities with too large an ionic radius have generally little chance to be introduced in the lattice, whereas small ions can find interstitial positions and create strong local distortion of the crystal electronic configuration.

In practice it is difficult, or at least very expensive, to purify raw materials to the sub-ppm level. Most of the scintillators grown in good conditions have therefore an impurity concentration of about 10^{-17}–10^{-19} cm^{-3}, comparable to the concentration of point defects.

3.3.2 Impact of Defects on Optical Properties

Defects in a crystal influence its optical properties in a number of ways, affecting the charge carriers or the photon transport.

3.3.2.1 Charge Carrier Traps

Most point defects or impurities are electron or hole traps. They reduce therefore the transfer efficiency of charge carriers to the luminescent centres and therefore also the scintillation efficiency. For good quality crystals the density of defects (at 1–100 ppm level) is several orders of magnitude smaller than the density of luminescent centres, which is very high for intrinsic scintillators (about 10^{22} cm^{-3}) but also quite high for extrinsic scintillators, for which the activator concentration is typically at the atomic percent level. Under normal excitation conditions, it would look therefore rather unlikely that charge carriers are trapped by defects before they convert on luminescent centres. This does not take into account the charge carrier capture cross-section, which can vary by large factors for different kinds of traps. A typical example is given by the molybdenum molecular complex MoO_4^{2-}, which is a very efficient and stable electron trap with a radiative decay at 508 nm in PWO. At the level of only a few ppm it gives rise to a slow (500 ns) additional green component to the regular fast PWO emission band at 420 nm. As molybdenum is isomorphic to tungsten it can easily enter into the PWO lattice and locally produce a solid solution ($PbWO_4$-$PbMoO_4$). This slow green component is negligible if the molybdenum contamination of the tungsten oxide raw material is less than 1 ppm [26].

In some cases, the traps are non-radiative but have energy levels close enough to the valence or conduction bands so that the carriers can be released by thermal activation, eventually converting on the luminescent centres. If the trap is close to the radiative centre this thermally assisted transfer can take place directly between them without involving the valence or conduction bands. As a result, the regular emission will take place but with some delay associated with the transit of the carrier via the trap. This is the origin of the well-known afterglow or phosphorescence. When afterglow effects are undesirable, for instance for high X-ray counting rates in CT scanners, additional impurities can help opening some non-radiative relaxation channels for these traps. As an example, afterglow in $(Y,Gb)_2O_3$:Eu scintillators can be significantly reduced by the addition of heterovalent Pr^{3+} or Tb^{3+} ions to the lattice [27]. The Pr^{3+} and Tb^{3+} additives readily trap holes to form Pr^{4+} and Tb^{4+}, which compete with the intrinsic traps responsible for afterglow. This energy trapped in the Pr or Tb sites decays non-radiatively in the presence of the Eu^{3+} ion. As a consequence, afterglow emission is suppressed by one order of magnitude or more.

3.3.2.2   Defect Associated Absorption Bands

Defects have generally energy levels in the forbidden band, which reduce the optical transparency of the crystal. Small perturbations of the crystal lattice are energetically the most probable ones and give rise to a number of energy levels near the conduction and the valence bands. There is nearly a continuum of such levels, which reduces the optical transparency window of the crystal. For this reason, the shape of the optical transmission of a crystal near the band-edge is usually a good probe of its structural quality. Crystals with UV emission bands near the fundamental absorption edge are strongly affected by the optical transitions between these levels resulting in increased absorption.

Cross-luminescent crystals such as Barium Fluoride (BaF_2) are illustrative examples to demonstrate the role of impurities on the crystal properties. Their deep UV fast emission band (220 nm for BaF_2) requires a very good UV transmission to detect efficiently the light at the photodetector. Unfortunately, alkali earth fluorides are easily contaminated by oxygen and hydroxyl ions, causing strong absorption bands in the UV. A theoretical study of the charge state stability and electronic structure of O^0, O^- and O^{2-} centres in BaF_2 identified a large number of transitions from 2p to 3s and 5s states. In ref. [28] Hartree-Fock-Slater local density discrete variation cluster calculations were made to obtain the energy levels of $H_s{}^-$, $O_s{}^-$ and $O_s{}^{2-}$ ions in BaF_2 crystals. Table 3.1 summarizes the optical absorption bands in the VUV and UV ranges.

As far as O^- and O^{2-} ions are concerned, the absorption bands are mainly the result of cross transitions between oxygen ions and Ba^{2+} or F^- ions, which significantly contribute to absorption around 200–240 nm.

These theoretical calculations are in good agreement with experimental results, confirming the existence of strong absorption bands overlapping the fast emission band in hydrolysed BaF_2 crystals, see Fig. 3.16.

Table 3.1 Calculated optical absorption band of H_s, $O_s{}^-$ and $O_s{}^{2-}$ -contaminated BaF_2 [28]

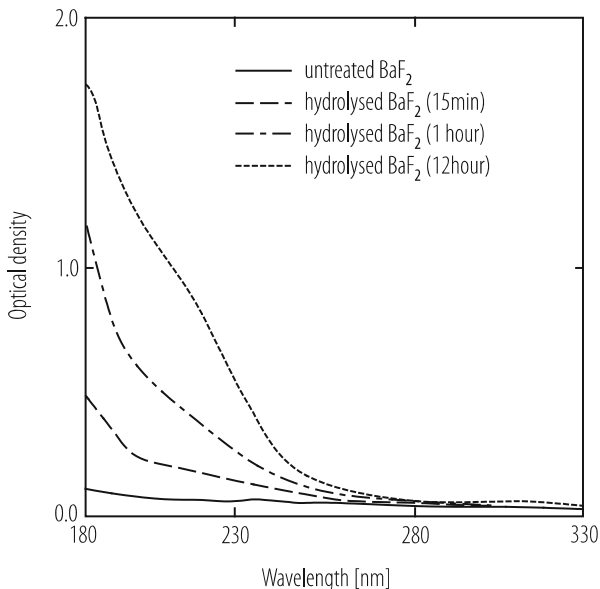| Impurities	λabs. [nm]	$h\nu$ [eV]	Cross transitions
$H_S{}^-$	209	5.9	H^- (1s) → H^- (2s)
$O_S{}^-$	230	5.4	F^- (2p) → O^- (2p,3p)
$O_S{}^{2-}$	175	7.2	F^- (2p) → O^- (3p)
	170 ≈ 175	7.0 ≈ 7.2	O^- (2p) → Ba^{2+} (5d)
	292	4.2	F^- (2p) → O^{2-} (3p)
	200	6.2	O^{2-} (2p) → Ba^{2+} (6s)
	130	9.5	O^{2-} (2p) → Ba^{2+} (5d)

Fig. 3.16 Absorption spectra for different hydrolysed BaF$_2$ (ref. [28])

3.3.3   Radiation Damage

The exposure of crystals to ionizing or neutron radiation can induce a number of modifications of the crystal lattice with potential consequences for the scintillation efficiency and the light transport. These modifications can be related to pre-existing crystal defects, when exposed to a high density of charge carriers that are easily trapped producing colour centres with radiation-induced absorption bands. They can also be associated to the production of new defects by elastic or knock-on collisions of incident particles with the lattice ions resulting in a local modification of the lattice structure. Finally, heavy energetic charged particles or neutrons may produce dramatic events, such as heavily ionizing fission fragments. This last phenomenon is usually of little concern in the majority of applications, even for the new generation of high luminosity particle physics colliders, as it requires an enormous integral fluence (10^{17}–10^{18} cm^{-2}) to become significant. Indeed, it requires the formation of about 10^{17} cm^{-3} such defects to reach a 1 ppm contamination in the majority of scintillator materials. However, such defects are by nature irrecoverable and their progressive accumulation may affect parts of detectors highly exposed for very long periods of time.

The situation is different for the majority of other cases (charge trapping or ion displacement), for which relaxation processes play a fundamental role in the kinetics of damage build-up. These defects introduce a local perturbation in the crystal and do not change the main structure parameters and particularly the spatial

symmetry group. However, they locally modify the electronic configuration and affect the macroscopic crystal parameters, such as optical transmission, conductivity, thermo-luminescence properties, because these volume properties are sensitive to the microscopic structure modifications. In ionic crystals, containing anions and cations, five possible simple point defects of the crystalline structure have been observed: anion vacancy V_a, cation vacancy V_c, cation replacement by impurity ions, extrinsic atoms in inter-site positions and Frenkel type defects (anions and cations displaced to interstitial sites).

All these defects are efficient charge carrier traps and can be stabilized by capturing excess electrons or holes released by irradiation in the conduction or valence band respectively. In oxide compounds for instance, the oxygen vacancies are charge compensated by the capture of one or two electrons, which are in excess in the conduction band after irradiation. The resulting F^+: $(V_a + e^-)$ and F: $(V_a + 2$ $e^-)$ electron centres play an important role in radiation damage effects. The captured electron or hole in these so-called recharged defects has generally a number of discrete energy levels available in the electrostatic environment of the defect and optical transitions to upper energy levels induce absorption bands in the crystal transparency window. These bands are the source of the crystal colouring under irradiation and justify the name of colour canters for these defects.

The main consequence of irradiating a crystal is to produce radiation induced absorption bands, which absorb a fraction of the scintillation light on its pathway to the photodetector. The light collected on the photodetector becomes therefore:

$$I_{rad} = \int_\lambda I_0(\lambda)\, e^{-(\mu_0(\lambda)+\mu_{rad}(\lambda))L} d\lambda \tag{3.15}$$

where I_{rad} is the intensity of the transmitted light after irradiation, $I_0(\lambda)$ is the intensity of transmitted light at the wavelength λ before irradiation, $\mu_0(\lambda)$ and $\mu_{rad}(\lambda)$ are, respectively, the intrinsic and radiation induced absorption coefficient at the wavelength λ and L is the mean path-length of optical photons from the emission point to the crystal exit surface. Dense and small radiation length crystals have an obvious advantage as for the same stopping power the path-length L is reduced as compared to lighter materials. Moreover, non-uniformities introduced by different path-lengths as a function of the position of the scintillation emission point are also reduced. Figure 3.17 shows the radiation induced absorption coefficient spectrum for PWO crystals as a function of the accumulated ^{60}Co dose.

At radiation levels currently experienced in particle physics detectors and in X-ray imaging devices the radiation damage only affects the optical transparency of the majority of known scintillators, but not the scintillation mechanism. One exception is CsI(Tl), characterized by an overlap of the radiation induced hole centres absorption maximum in CsI with the excitation spectrum of the Tl^+ ions. The presence of stable hole centres causes a fraction of excitations to be trapped rather than transferred to Tl^+ thereby causing non-radiative losses. As a result, the efficiency of energy transfer to luminescence centres drops, decreasing the scintillation efficiency. Similarly, radiation-induced charge transfer processes can
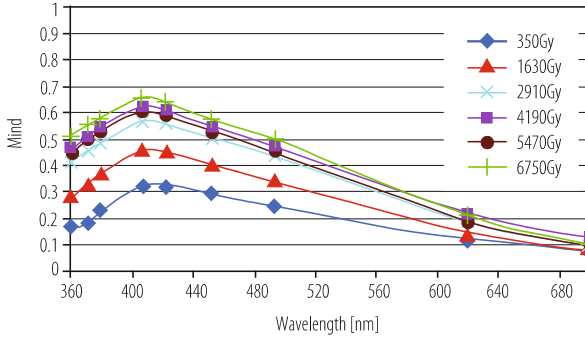
Fig. 3.17 Wavelength dependent absorption coefficient of PWO crystals as a function of the absorbed ^{60}Co dose (courtesy CMS collaboration)

modify the charge state of activator ions. This is seen for instance in some Ce^{3+} doped scintillators, such as YAP and LuYAP, when grown in vacuum or inert atmosphere, where up to several percent of the scintillating Ce^{3+} ions can be reduced under irradiation to the Ce^{2+} non-scintillating state, decreasing by the same amount the scintillation efficiency. Annealing the crystals under oxygen atmosphere restores the scintillation efficiency by re-oxidizing the Ce^{2+} ions. Ref. [11] provides more details.

The kinetics of the radiation damage build-up and recovery is determined by the depth of the traps at the origin of colour centres. Very shallow traps induce transient absorption bands, which recover so quickly that the monitoring of the crystal transparency becomes very difficult. Much attention has been paid when optimizing PWO crystals for the CMS calorimeter at LHC to suppress as much as possible such defects or to compensate their effect by specific doping [8, 29]. On the other hand, deep traps are generally very stable and are characterized by a continuous increase of the corresponding absorption bands, even at low dose rate, until they are completely saturated. The monitoring of the crystal transparency allows correcting for light yield variations but the concentration of such defects must be maintained small enough to minimize the loss in light yield. For most of the known scintillators a concentration of such defects at the ppm level can produce a radiation induced absorption coefficient limited to about 1 m^{-1}.

At room temperature a large fraction of the radiation induced defects are metastable. Temperature dependant relaxation processes take place in the crystal lattice so that these defects, once produced, are ionized at a rate, which depends on their energy depth and the temperature following the Boltzmann law. As a consequence, the transmission damage reaches a saturation level, which is dose-rate-dependent up to the point where the rate of trapping of the charge carriers induced by radiation is exactly balanced with the rate of spontaneous relaxation at this working temperature. For a uniform distribution of defects of type i in the crystal

and in the absence of an interaction between them the kinetics of the concentration of damaged centres of type i is described by the following differential equation:

$$\frac{\mathrm{d}N_i}{\mathrm{d}t} = -\omega_i N_i + \frac{S}{d_i}\left(N_i^* - N_i\right) \tag{3.16}$$

where N_i is the amount of damaged centres of type i at time t, ω_i is their recovery rate, S is the dose rate, N_{i*} is the amount of pre-existing defects of type i and d_i is a damage constant, which depends on the capture cross-section of free carriers by the centres of type i. The induced absorption coefficient μ produced by irradiation is proportional to the concentration of absorbing centres N through $\mu = \sigma N$, where σ is the cross-section of the absorbing centre. The solution of this equation gives the kinetics of the induced absorption build-up:

$$\mu = \mu_{\mathrm{sat}}\frac{S}{S + \omega d}\left\{1 - \exp\left[-\left(\omega + \frac{S}{d}\right)t\right]\right\} \tag{3.17}$$

where $\mu_{sat} = N_*\sigma$ corresponds to the maximum possible saturation when all centres are damaged. The recovery of the transmission after the end of the irradiation at time t_0 is described by:

$$\mu = \mu_{\mathrm{sat}}\frac{S}{S + \omega d}\left\{1 - \exp\left[-\left(\omega + \frac{S}{d}\right)t_0\right]\right\}\exp\left(-\omega\left(t - t_0\right)\right) \tag{3.18}$$

Figure 3.18 illustrates the impact of this behaviour on the light output of a 23 cm long PWO crystal exposed to a cycle of several irradiations separated by periods of recovery.

There are two ways to increase the radiation hardness of scintillating crystals. The first one is to make every effort to reduce the density of point charge defects
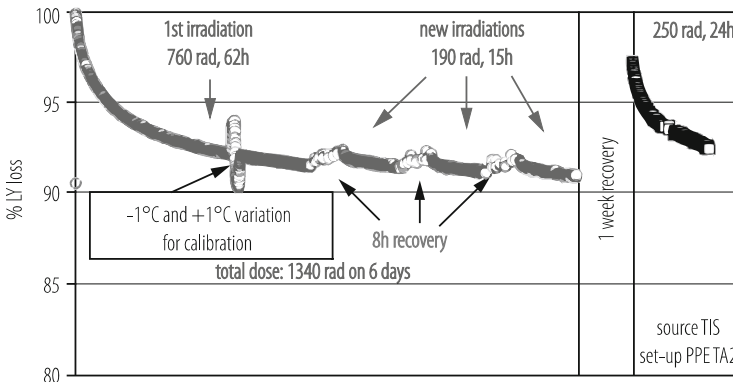
Fig. 3.18 Variations of light out-put for a PWO crystal exposed to a cycle of several irradiations separated by periods of recovery at 18°C (courtesy CMS collaboration)

related to structural defects, impurities and anion or cation vacancies induced by differential evaporation of the chemical components during the crystal growth. This can be achieved for the majority of crystals, through different cycles of purification of the raw materials, multiple crystal growth and annealing of the crystals in specific atmosphere and temperature conditions. This approach is however costly and limited to defect concentration levels in the ppm range. For some applications, such as in high luminosity collider experiments, this is sometimes not enough to guarantee the optical stability of the crystals over long periods.

In another approach additional well selected defects are produced in the crystal, which compete with the uncontrollable defects and reduce their influence. This so-called co-doping strategy has been the result of improved understanding of the mechanisms of light production and charge carrier transport and trapping, opening the way to a defect engineering of the crystals. It has been shown for instance that divalent doping with Ca^{2+} or Mg^{2+} in some Ce^{3+} activated crystals (in particular in ortho-silicates and aluminium garnets), not only increases the light yield, but also suppresses slow scintillation components and improves the radiation hardness [30]. This is the result of easier charge carrier transport to the luminescent centres through the energy levels of these impurities and easier delocalization of trapped carriers due to the smaller energy gap between these traps and the conduction band, which may even absorbed in the conduction band.

3.4 Crystal Engineering. Impact of New Technologies

The conditions of synthesis of the chemical components of a crystal are governed by thermodynamic relations between composition, temperature and pressure of the mixture. At a given pressure, the composition-temperature equilibrium for both the liquid and solid phases is represented by a phase diagram. The phase diagram shows the domains of stability of a given chemical composition and the influence of deviations from stoichiometry (composition of the mixture), unwanted impurities or specific doping. An example of such a phase diagram is shown in Fig. 3.19 for PWO crystals.

Two stable compositions can be grown from a PbO-WO_3 mixture, namely $PbWO_4$ (PWO) and Pb_2WO_5. The $PbWO_4$ melts congruently, i.e. without decomposition of the compound, at $1123°C$. The analysis of this phase diagram helps to define some practical parameters for the $PbWO_4$ crystals. First of all the melting temperature restricts the choice of the crucibles to metals with melting points much higher than $1123°C$, such as platinum, iridium and their various alloys. Moreover, such crucibles must be chemically inert with melts of similar oxides like $PbMoO_4$, $CaMoO_4$, $ZnWO_4$, as Mo, Ca and Zn are impurities likely to be present in the raw materials. Secondly, the possibility to deviate from the perfect stoichiometric composition of the raw material with some excess of either WO_3, or PbO is of great importance to compensate for a strong differential evaporation of the different components of the melt during the growth process. An initial deviation
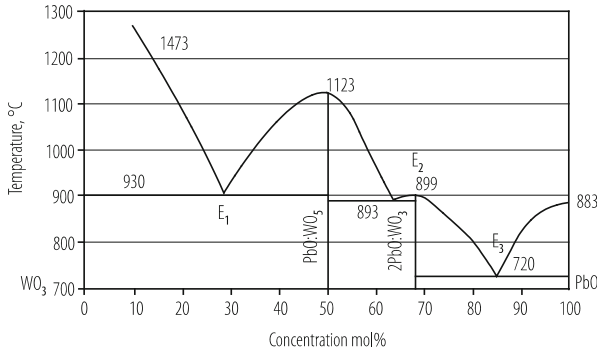
Fig. 3.19 Phase diagram of the PbO-WO$_3$ system

from the perfect stoichiometry can compensate non-stoichiometry defects. Some restrictions can appear because of segregation processes of additional doping ions. The segregation coefficient k defines how the concentration of doping ions or impurities will vary along the crystal according to the formula:

$$C_s = \frac{kC_0}{1 - (1 - k)\,g} \tag{3.19}$$

where g is the fraction of the melt already crystallized, C_S is the impurity concentration in the melt at some point, C_0 is the initial impurity concentration in the melt, k is the segregation coefficient. If the segregation coefficient k is too different from 1, as a result of too small or too large ionic radii or different valence states as compared to the ions of the crystal lattice, the doping ion will be pumped in or repelled from the crystal during the growth process.

The majority of crystal growth methods are based on the principle of oriented crystallization. An oriented seed (a small piece of the same crystal or of different composition but similar lattice parameters) is introduced in contact with the melt to initiate the growth process. A temperature gradient is applied so that heat transfer is used as the driving force of crystallization. Several crystallization methods have been developed, which differ in the way the heat transfer and the hydrodynamic conditions are applied:

- Establishing a temperature gradient between the crystal and the melt by heat transfer from the seed. Such heat transfer methods occurred in nature to form crystals and are still used for cheap crystal production, when the requirements on quality are not too high.
- Floating temperature gradient through the melt (Bridgeman and Stockbarger methods). The raw material is placed in a closed crucible, at the end of which a seed has been placed. The crucible is moved through a thermal gradient zone, where the temperature is lowered below the melting point. This is the area where the crystallization takes place. The volume of the melt will therefore decrease

continuously and the growing crystal starts substituting for the melt. This method is relatively inexpensive and multiple crystal pulling is possible by moving several crucibles together through the temperature gradient zone of a single oven [31]. If the simplicity and reliability of the Bridgeman and Stockbarger methods make them particularly attractive for many applications, these methods suffer from several drawbacks, such as large variations of the temperature field parameters during the crystal growth and strong non-uniformities in the distribution of doping ions, impurities and defects in the crystal.

- Establishing a temperature gradient between the crystal and the melt in an open crucible by progressive cooling of the melt after seeding or extracting the growing crystal from melt (Kyropoulos and Czochralski methods, respectively). In the classical Kyropolos method [32] the entire crystallization process starts with the seeding and propagates through the melt as a result of a continuous temperature decrease applied during the process. There is no relative movement of the seed and the crucible. In the Czochralski method [33] the crystal is pulled from the melt. The seed is attached to a Platinum rod and put in contact with the melt in the crucible. The rod or the crucible (sometimes both) are rotating at a few rpm to maintain a good homogeneity of the melt in contact with the crystallized phase. The rod is simultaneously pulled up at a speed of typically 1–10 mm/h depending on the crystal. This method is the most widely used for growing oxide scintillators and several other types of scintillators because of its potential to grow high quality crystals by concentrating impurities and defects in the bottom part of the crucible.

More details about crystal engineering techniques are given in ref. [11].

Technologies for the production of crystals are rapidly evolving. The impressive progress in nanotechnologies in particular open new perspectives for the production of pre-reacted raw materials of excellent quality with a high uniformity of the grain sizes. With these new materials, transparent ceramics of heavy scintillators can be produced (Fig. 3.20), with the advantage over standard crystal growth techniques to be much more cost effective: not only the scintillator can be produced to its final shape, saving on the cost of mechanical processing, but also the temperature for sintering is usually much lower than for standard crystal growth.

The recently developed pulling-down technology from a shape-controlled capillary die gives the possibility to produce elongated crystals with dimensions that are not accessible using traditional cutting and polishing of bulk crystals grown by the more standard Czochralski or Bridgeman methods (Fig. 3.21). This approach has important advantages, such as growing the crystal in the final shape (round, oval, square, rectangular, hexagonal), very rapidly (several millimeters per minute instead of millimeters per hour), simultaneous multifibre pulling, increased activator doping concentration, etc. Excellent quality BGO, YAG and LSO fibers have been grown with a length of up to 2 m and a diameter between 0.3 and 3 mm. Some other materials are being studied, in particular from the very interesting perovskite family: YAP and LuAP [34].
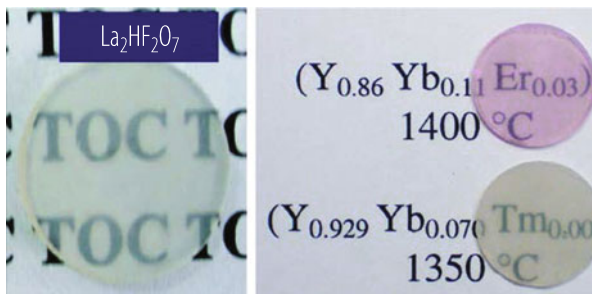
Fig. 3.20 Transparent ceramics of different heavy scintillators prepared with pre-reacted nanopowders
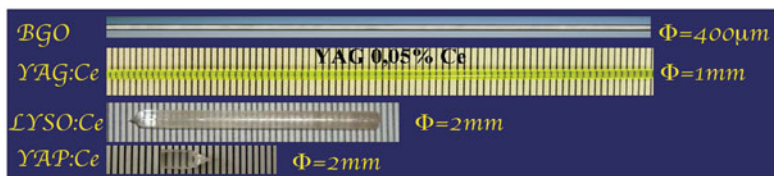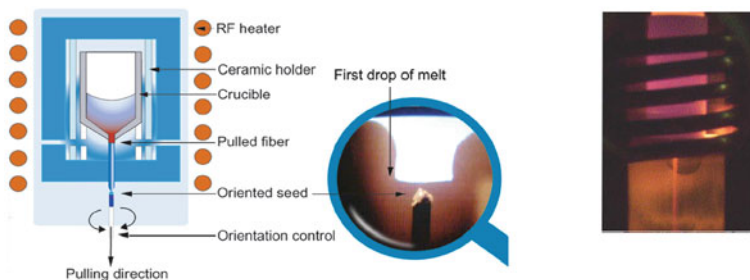
Fig. 3.21 The micro-pulling down crystal growth technology (courtesy Fibercryst)

3.5 Table of Commonly Used Scintillators

Inorganic scintillators generally considered for a majority of applications, and in particular, for particle physics detectors and medical imaging cameras are listed in Table 3.2 with their most important physico-chemical and optical properties. A much more exhaustive list of scintillators classified according to their chemical structure is presented in ref. [11].

Table 3.2 Most commonly used scintillators with their main physico-chemical and optical parameters

Scintillator	Simplified name	Density [g/cm^3]	Light Yield [ph/MeV]	Emission wavelength [nm]	Decay time [ns]	Hygro-scopic	Main application
NaI :Tl		3.67	38,000	415	230	Yes	Medical imaging, industrial γ camera, homeland security
CsI :Tl		4.51	54,000	550	1000	Lightly	Physics detectors
CdWO$_4$	CWO	7.9	28,000	470/540	20,000/5000	No	X-Ray scanner
(Y,Gd)$_2$O$_3$:Eu	YGO	5.9	19,000	610	1000	No	X-Ray scanner
Gd$_2$O$_2$S:Pr,Ce,F	GOS	7.34	21,000	520	3000	No	X-Ray scanner
Bi$_4$Ge$_3$O$_{12}$	BGO	7.13	9000	480	300	No	Physics detectors medical imaging
Gd$_2$SiO$_5$	GSO	6.7	12,500	440	60	No	Medical imaging
Lu$_2$SiO$_5$	LSO	7.4	27,000	420	40	No	Medical imaging
Lu$_2$AlO$_3$	LuAP	8.34	10,000	365	17	No	Medical imaging
LaBr$_3$:Ce	BriLanCe™	5.29	61,000	358	35	Very	Medical imaging
BaF$_2$		4.89	2000/8000	220/310	0.7/620	No	Physics detectors
CeF$_3$		6.16	2400	310/340	30	No	Physics detectors
PbWO$_4$	PWO	8.28	200	420	5/15	No	Physics detectors

References

1. B. Rossi, High Energy Particles, Prentice-Hall, Inc. Englewood Cliffs, NY, 1952.
2. U. Fano, Annu. Rev. Nucl. Sci. 13 (1963) 1.
3. J.D. Jackson, Classical Electrodynamics, 2nd ed., Wiley, New York, 1975, chap. 13.
4. R.D. Evans, The Atomic Nucleus, Krieger, New York, 1982.
5. A. Lempicki et al., *Fundamental limits of scintillator performance*, Nucl. Instrum. Meth. A 333 (1993) 304-311.
6. P. Lecoq et al., *Lead Tungstate (PbWO₄) scintillators for LHC EM calorimetry*, Nucl. Instrum. Meth. A 365 (1995) 291-298.
7. Scintillation Detectors, Catalog, Saint Gobain, Ceramiques Industrielles, March 1992.
8. A. Annenkov et al., *Suppression of the radiation damage in Lead Tungstate scintillation crystal*, Nucl. Instrum. Meth. A 426 (1999) 486-490.
9. The CMS Collaboration (2015) Technical proposal for the phase II upgrade of the compact muon solenoid, CERN-LHCC-2015-010/LHCC-P-008
10. Gundacker S. et al, (2013), Time of Flight positron emission tomography towards 100ps resolution with L(Y)SO: an experimental and theoretical analysis, JINST 8:P07014
11. P. Lecoq, A. Annenkov, A. Gektin, M. Korzhik, C. Pedrini, Inorganic Scintillators for Detector Systems, Springer-Verlag, 2006. Second edition 2017, ISBN 978-3-319-45521-1 doi 10.1007/978-3-319-45522-8
12. A.J. Dean, *Imaging in high-energy astronomy*, in: *Heavy Scintillators for scientific and industrial applications*, Proc. Int. Workshop Cristal 2000, Sep 22-26, 1992, Chamonix, France, F. De Notaristefani, P. Lecoq, M. Schneegans (eds.), Editions Frontières France, 1992, pp. 53-64.
13. C. Kuntner et al., *Intrinsic energy resolution and light output of the Lu0.7Y0.3AP:Ce scintillator*, Nucl. Instrum. Meth. A 493 (2002) 131-136.
14. M.C. Abreu et al., *ClearPEM: A PET imaging system dedicated to breast cancer diagnostics*, Nucl. Instrum. Meth. A 571, (2007) p. 81-84.
15. J.B. Birks, The Theory and Practice of Scintillation Counting, Pergamon, London, 1964.
16. A. Vasiliev, *Relaxation of hot electronic excitations in scintillators: account for scattering, track effects, complicated electronic structure*, Proc. Fifth Int. Conf. Inorganic Scintillators and their Applications, SCINT99, V.V. Mikhailin (ed.), Moscow State University, Moscow, 2000, pp. 43-52.
17. C. Pedrini et al., *Time-resolved luminescence of CeF₃ crystals excited by X-ray synchrotron radiation*, Chem. Phys. Lett. 206 (1993) 470–474.
18. M. Kronberger, E. Auffray, P. Lecoq, *Probing the concept of Photonics Crystals on Scintillating Materials*, Proc. 9th Int. Conf. Inorganic Scintillators and their Applications, Winston-Salem, NC, June 4-8, 2007, IEEE Trans. Nucl. Sci. 55(3) (2008) 1102-1106.
19. A. Knapitsch, P. Lecoq, Review on photonic crystal coatings for scintillators, International Journal of Modern Physics A, Vol. 29 (2014) 1430070 (31 pages) https://doi.org/10.1142/S0217751X14300701
20. R.B. Murray, A. Meyer, *Scintillation response of activated inorganic crystals to various charged particles*, Phys. Rev. 122 (1961) 815-826.
21. W.W. Moses, S.A. Payne, W.S. Choong, *Scintillator Non-Proportionality: Present Understanding and Future Challenges*, IEEE Trans. Nucl. Sci. 55(3) (2008) 1049-1053.
22. B.D. Rooney, J.D. Valentine, *Scintillator Light Yield Non-proportionality: Calculating Photon Response Using Measured Electron Response*, IEEE Trans. Nucl. Sci. 44(3) (1997) 509-516.
23. P. Lecoq, M. Korzik, A. Vasiliev, *Can transient phenomena help improving time resolution in scintillators?*, IEEE Trans. Nucl. Sciences, Vol. 61, NO. 1, February 2014
24. J.Q. Grim et al., *Continuous-Wave Biexciton Lasing at Room Temperature Using Solution-Processed Quantum Wells,* Nat. Nanotechnol. **9,** 891–895 (2014)
25. P. Lecoq, *Metamaterials for novel X- or γ-ray detector designs*, 2008 IEEE Nuclear Science Symposium Conference Record, N07-1, pp.680-684

26. A. Annekov, M. Korzhik, P. Lecoq, et al., *Slow components and afterglow in PWO crystal scintillation*, Nucl. Instrum. Meth. A 403 (1998) 302-312.
27. US Patent 5521387
28. Chen Lingyan, Du Jie, Wang Liming, Xiang Kaihua, *An investigation of radiation damage induced by hydroxyl and oxygen impurities in BaF2 crystal*, Scintillator and Phospor Materials MRS Proceeding 348 (1994) 447-454.
29. A. Annenkov, M. Korzhik, P. Lecoq, *Lead tungstate scintillation material*, Nucl. Instrum. Meth. A 490 (2002) 30–50.
30. M. Nikl et al., *Defect Engineering in Ce-Doped Aluminum Garnet Single Crystal Scintillators,* Cryst. Growth Des. 2014, 14, 4827−4833, dx.doi.org/10.1021/cg501005s
31. Z.W. Yin, Q. Deng, D.S. Yan, *Research and Development Works on PbWO4 Crystals in Shanghai Institute of Ceramics*, Proc. 5th Int. Conf. Inorganic Scintillators and their Applications, Moscow, Apr 16-20, 1999, pp. 206-211.
32. S. Kyropolos, F. Zeits, *Ein Verfahren zur Herstellung grosser Kristalle*. Anorg. Allgem. Chem. 154 (1926) 308–313.
33. J. Czochralski, *Ein neues Verfahren zur Messung der Kristallisationsgeschwindigkeit der Metalle*, Z. Phys. Chem. 92 (1918) 219-224.
34. B. Hautefeuille et al., J. Crystal Growth 289 (2006) 172.